The Pennsylvania State University

The Graduate School

Department of Chemical Engineering

ACCELERATED MOLECULAR DYNAMICS SIMULATION OF THERMAL DESORPTION

A Dissertation in

Chemical Engineering

by

Kelly E. Becker

Submitted in Partial Fulfillment
of the Requirements
for the Degree of

Doctor of Philosophy

December 2008

The dissertation of Kelly E. Becker was reviewed and approved* by the following:

Kristen A. Fichthorn
Professor of Chemical Engineering
Professor of Physics
Dissertation Advisor
Chair of Committee

Seong H. Kim
Associate Professor of Chemical Engineering

Janna K. Maranas
Associate Professor of Chemical Engineering

Milton W. Cole
Distinguished Professor of Physics
Distinguished Professor of Materials Science and Engineering

Andrew L. Zydney
Professor of Chemical Engineering
Head of the Department of Chemical Engineering

*Signatures are on file in the Graduate School

ABSTRACT

Desorption is a process ubiquitous in phenomena involving surfaces. However, it has rarely been simulated on the molecular level. Molecular dynamics simulation can provide the atomic-level detail necessary to study desorption on the molecular level but has limitations on the time scales that can be simulated. We present a set of accelerated molecular dynamics methods that can be used to simulate desorption of alkanes from the basal plane of graphite (a process that occurs over the time scale of seconds or minutes) with atomic level detail. Single molecule simulations, accelerated by increasing the temperature of the simulation, shed light on conformational changes that occur in alkane molecules on the graphite surface. These temperature accelerated simulations are compared to a compensating potential method for the single molecule so that the simulations can be extended to finite coverage. We present finite coverage simulations for the desorption of pentane from the basal plane of graphite. Desorption environments are characterized, and the presence of entropy-driven desorption is discovered. Ultimately, the accelerated simulations are extended to simulate temperature-programmed desorption experiments. We find that analyzing the results as in experimental literature fails to predict some of the features in the temperature programmed desorption profiles. Suggestions are made for further characterization of the desorption process.

TABLE OF CONTENTS

LIST OF FIGURES

LIST OF TABLES

ACKNOWLEDGEMENTS

To quote the Grateful Dead, “Lately it occurs to me: What a long, strange trip it’s been.” I never imagined when I started graduate school that this is what my life would be when I graduated. But I’ve enjoyed the trip (however strange) and now I get the chance to thank the people who have journeyed with me.

First and foremost, a great big thanks goes to Kristen. Your passion for research and knowledge is unparalleled and infectious. You’ve taught me to be a good researcher and to always question. I wouldn’t be the engineer that I have become without your guidance. Thank you to the other members of my committee: Seong Kim, Janna Maranas and Milton Cole. I appreciate the time that you have taken to read my papers, listen to my presentations, and give constructive comments.

I have made wonderful friends in my time in State College. Thank you to Derek and Maria for all the adventures and fun. Tim and Karen have been more generous than I could have ever asked and for that I am extremely grateful. They gave this interstate traveler a place to lay her weary head, opened their house to me, and provided some of the most enlightening conversations about life, the universe and everything.

Old friends are truly life’s treasures, and I have had one of the best cheering me on as I worked on my thesis. Whatever I needed, encouragement or a good laugh or an ear to listen to me complain, my brother has always been there for me.

In a recent Time magazine, Claudia Wallis wrote “We never forget our best teachers – those who imbued us with a deeper understanding or an enduring passion, the ones we come back to visit years after graduation, the educators who opened doors and

altered the course of our lives." I am supremely lucky to have met more than one teacher like this. They helped to start me on this path and so I share the joy of this accomplishment with them.

Of course, the best teachers in life are our first teachers. My parents have supported me in everything that I have done, in every way possible. I couldn't ask for better ones. They have probably forgotten more molecular simulation than they ever thought they would learn, but still they have read every paper and listened to all the presentations. They taught me the value of hard work, and my father has always been my model of what an engineer should be.

Last, but certainly not least, I have to thank my husband, Justin. I doubt either one of us thought this is where life would lead when we met that very first time as graduate students. He has shown unwavering patience and love throughout this whole journey. Thank you for everything.

Chapter 1

Introduction

Desorption is a fundamental process in many applications including catalysis, assembly at surfaces, wetting, etching, and thin-film growth. Extensive research has been conducted to characterize the desorption process of both atoms and molecules from a variety of surfaces. A complete understanding of the desorption process can be obtained by examining the molecular environments during desorption. However, limitations of space and time resolution prohibit such understanding from experiments. Molecular dynamics (MD) simulations can provide the necessary molecular-level detail. Such simulations present their own time resolution issues. In MD simulations, the time step of the simulation is limited by the fastest movement in the system and leads to time steps on the order of femtoseconds (fs). This limits the simulation time to the order of nanoseconds. At experimentally relevant conditions, the desorption process occurs over seconds or even minutes. To bridge this time gap, accelerated MD methods based on hyperdynamics [**1-4**] are applied to the desorption problem. This in turn allows the simulation of the time scale necessary to observe desorption events, while still providing molecular-level detail.

1.1 Temperature Programmed Desorption (TPD)

Temperature programmed desorption (TPD) is a powerful experimental tool used to study the desorption of alkanes from a variety of surfaces [**5-10]**. The analysis of TPD experiments is based on an Arrhenius expression for the desorption process

$$k = \nu \exp\left(-E_D / k_B T\right) \qquad \textbf{1.1}$$

where k is the desorption rate constant, ν is the prefactor, E_D is the desorption energy, k_B is Boltzmann's constant, and T is the temperature. The two parameters that determine the characteristics of the desorption process are the prefactor and the desorption energy. In recent research, there has been much discussion about how the prefactor relates to the chain length of alkane molecules [**5-7,9-11**]. Although the adsorption of alkane molecules on various surfaces is thought to be dominated by physical forces that are independent of the characteristics of the surface, prefactors calculated in studies from gold [**7**], graphite [**5,10,11**], platinum [**6**,**10**], and magnesium oxide [**9**] show prefactors that differ by six orders of magnitude. In addition, some of the studies [**7,9-11**] show a prefactor that increases with increasing chain length. Others [**5,6**] show the opposite, a prefactor that is constant with increasing chain length.

These discrepancies may arise from any of a number of different factors or some combination. It is possible that there is a fundamental difference between alkane desorption from metallic and non-metallic surfaces. However, it has been reported that the prefactor may increase [**10,11**] or remain constant [**5**] on a graphite surface. It has also been reported that the prefactor increases on both metallic [**7**] and non-metallic [**9,10**] surfaces. As such, this explanation is unlikely. A second factor is a fundamental

difference between the molecules that are being studied. An experimental study of short alkane desorption from a graphite surface [**10**] shows a prefactor that increases with increasing chain length. Another experimental study [**5**] of much longer alkane chains shows a prefactor that is constant with increasing chain length. We provide a physical explanation that reconciles these inconsistent results [**11**]. A third explanation is that the analysis of experimental data from TPD is based on flawed assumptions. Such data are interpreted based on the assumption that desorption is a first-order process and that desorption energy and prefactor are independent of coverage. The work presented herein shows that this is not the case, and recommendations are given for re-evaluating the assumptions.

1.2 Ordering and Orientation

Given that the desorption process is not independent of coverage, it is important to examine ordering and orientation of alkane molecules on graphite surfaces. This provides insight into possible desorption environments. The configurations that a molecule takes on the surface affect not only the molecule-surface interaction but also the interaction that a molecule has with neighboring alkane molecules. These changing desorption environments influence both the desorption energy (as a combination of molecule-surface and intermolecular energy) and the prefactor (as a measure of the entropy gained following desorption). Many experimental [**12-15**] and simulation [**16-19**] studies have considered changes in environment with temperature. At low temperatures, alkane molecules lie flat with the plane of their backbones parallel to the

surface [**15,17**]. As the temperature is increased, molecules tip in either of two ways. At high coverages (those approaching a monolayer), molecules tip so that the long axis of the molecule is pointed out of the plane of the surface [**16**]. Molecules also roll so that the plane of the carbon backbone is perpendicular to the surface [**18**]. Both movements change the orientation of the alkane molecule relative to other alkane molecules in the layer, thus altering the desorption energetics. Moreover, desorption of alkane molecules from graphite occurs at temperatures higher than the melting point of alkane monolayers in the same system [**15,19**]. As a result, the highly structured monolayers that are observed in experiment [**14,15**] are not the same configurations that occur during desorption. Instead, desorption occurs from a liquid state.

1.3 Thesis Overview

This thesis presents a logical progression of desorption simulations. Chapter 2 introduces the methodology that is common to the simulations. This includes potential energy functions, simulation control measures such as constraint dynamics and temperature control, variables used to compare conventional MD simulations to accelerated simulations, and the general components of transition-state theory and acceleration schemes. Chapter 3 utilizes the concepts introduced in Chapter 2 to simulate the desorption of alkanes from the basal plane of graphite at the zero-coverage (single molecule) limit. Alkane chain length is varied from pentane to hexadecane to examine the effect that chain length has on the desorption energetics. Chapter 4 extends the simulation to a finite coverage and examines the structure of a pentane layer on the basal

plane of graphite. These conventional MD simulations validate the potential energy functions for use with this system by matching simulated quantities to experimental results [**15**]. Once the potential energy functions have been verified, they are used in the variable coverage simulations found in Chapter 5. These simulations of the desorption of pentane from the basal plane of graphite examine the role of entropy on the desorption process and address the limitations of zero-coverage simulations. Ultimately, in Chapter 6, the process of simulating desorption from a finite coverage is extended to an experimental system, namely a temperature programmed desorption (TPD) experiment. TPD simulations are performed at variable initial coverage and variable heating rate. These data are then analyzed in the same manner as experimental TPD data. The application of Redhead analysis [**20**] to the desorption of alkanes from graphite is discussed and conclusions are drawn about its applicability.

Chapter 2

Simulation Methodology

2.1 Molecular Dynamics

Molecular dynamics (MD) is a method used to simulate dynamic events and properties with atomic-level detail. It is based on Newton's second law relating the force acting on each atom to the acceleration that atom exhibits.

$$F_i = m_i \ddot{r}_i \qquad \textbf{2.1}$$

where F_i is the force acting on atom i, m_i is the mass of atom i, r_i is the position of atom i, and the dots above r_i indicate the second derivative with respect to time.

Each atom is treated as a classical particle, and the force is calculated as the first derivative of potential energy with respect to each coordinate x, y, and z. The expressions for the potential energy as a function of position are discussed in Section 2.2. Eq. **2.1** can be integrated assuming a constant force over a very small time step to obtain an expression for the velocity of each atom

$$\dot{r}(t + \Delta t) = \dot{r}(t) + \ddot{r}(t)\Delta t \qquad \textbf{2.2}$$

where Δt is the time step. It follows from Eq. **2.1**, the expression for the velocity can be expressed in terms of the forces acting on each atom as

$$\dot{r}(t + \Delta t) = \dot{r}(t) + \frac{F}{m}\Delta t \qquad \textbf{2.3}$$

Integrating Eq. **2.1** a second time gives an expression for the position of the atom based on the position and velocity at the previous time step

$$r(t+\Delta t) = r(t) + \dot{r}(t)\Delta t + 0.5\ddot{r}(t)\Delta t \qquad \textbf{2.4}$$

Again, Eq. **2.1** can be applied to obtain an expression for the position of an atom based on the forces acting on that atom

$$r(t+\Delta t) = r(t) + \dot{r}(t)\Delta t + 0.5\frac{F}{m}\Delta t \qquad \textbf{2.5}$$

The algorithm for MD calculations proceeds as follows:

1. Forces acting on each atom are calculated based on the current position of the atoms and the derivatives of the expressions for the potential energy between atoms.
2. Positions of all atoms are advanced according to Eq. **2.5**.
3. Velocities of all atoms are advanced according to Eq. **2.3**.
4. The resulting positions and velocities become the current positions and velocities for the next timestep.

Modifications to this generic algorithm to include constraints will be discussed in Section 2.3. Through successive application of the algorithm described above, trajectories in phase space are created. From these trajectories, one can calculate equilibrium and dynamic properties of the system of study.

2.2 Potential Energy Functions

2.2.1 Intramolecular Interactions

Each alkane molecule is modeled using an all-atom representation. This gives each molecule 3N degrees of freedom, where N is the number of atoms in the molecule. Three of these degrees of freedom account for rigid-body translation of the molecule, and three account for rigid-body rotation. The other 3N-6 degrees of freedom are internal degrees of freedom which include bond stretches, bond angle bends (3-body interactions), and torsion angle rotations (4-body interactions). The highest frequency modes (bond stretches and hydrogen-carbon-hydrogen angle bends) are constrained using the RATTLE algorithm, which will be discussed in Section 2.3. All other internal degrees of freedom are included in the potential energy field and are modeled as in the OPLS force field as follows [**21**].

$$U_{\text{int}ra} = U_\theta(\theta) + U_\varphi(\varphi) + U_{LJ}(r) \qquad \textbf{2.6}$$

$$U_\theta = \sum_i K_{\theta_i}\left(\theta_i - \theta_{eq}\right)^2 \qquad \textbf{2.7}$$

$$U_\varphi = \sum_i \frac{V_1^i}{2}\left[1+\cos(\varphi_i)\right] + \frac{V_2^i}{2}\left[1-\cos(2\varphi_i)\right] + \frac{V_3^i}{2}\left[1+\cos(3\varphi_i)\right] \qquad \textbf{2.8}$$

$$U_{LJ} = \sum_i \sum_j 4\varepsilon_{ij}\left[\left(\frac{\sigma_{ij}}{r_{ij}}\right)^{12} - \left(\frac{\sigma_{ij}}{r_{ij}}\right)^{6}\right] f_{ij} \qquad \textbf{2.9}$$

The angle bending potential, U_θ, is quadratic in the bend angle, θ_i, with a force constant K_θ for each type of bond angle. Values for K_θ and θ_{eq} are listed in Table **2-1**. The potential energy for four-body torsion angle rotations is modeled as a Fourier cosine series. In the OPLS formulation, each torsion angle is included explicitly instead of

assuming symmetry. Parameters for each type of torsion angle can be found in Table **2-1**. Non-bonded interactions are modeled using a Lennard-Jones 12-6 potential. The factor f_{ij} is added to differentiate 1-4 non-bonded interactions ($f_{ij} = 0.5$) from longer range non-bonded interactions ($f_{ij} = 1.0$). Values for ε_{ij} and σ_{ij} can be found in Table **2-1**. Cross parameters are calculated using standard Berthelot combining rules.

Table **2-1**: Potential Energy Parameters for Intramolecular Interactions

Parameter	Value	Units
K_θ (C-C-C)	58.35	Kcal/mol
K_θ (C-C-H)	37.50	Kcal/mol
θ_{eq} (C-C-C)	112.7	Degrees
θ_{eq} (C-C-H)	110.7	Degrees
V_1 (H-C-C-H)	0.000	Kcal/mol
V_1 (H-C-C-C)	0.000	Kcal/mol
V_1 (C-C-C-C)	1.740	Kcal/mol
V_2 (H-C-C-H)	0.000	Kcal/mol
V_2 (H-C-C-C)	0.000	Kcal/mol
V_2 (C-C-C-C)	-0.157	Kcal/mol
V_3 (H-C-C-H)	0.318	Kcal/mol
V_3 (H-C-C-C)	0.366	Kcal/mol
V_3 (C-C-C-C)	0.279	Kcal/mol
ε_{CC}	0.066	Kcal/mol
ε_{HH}	0.030	Kcal/mol
ε_{CH}	0.044	Kcal/mol
σ_{CC}	3.500	Å
σ_{HH}	2.500	Å
σ_{CH}	3.000	Å

2.2.2 Intermolecular Interactions

For simulations involving multiple alkane molecules, intermolecular interactions are necessary. In these simulations, they are modeled using a Lennard-Jones 12-6 functional form

$$U_{LJ} = \sum_{i} \sum_{j>i} 4\varepsilon_{ij} \left[\left(\frac{\sigma_{ij}}{r_{ij}} \right)^{12} - \left(\frac{\sigma_{ij}}{r_{ij}} \right)^{6} \right] f_{ij} \qquad \textbf{2.10}$$

where f_{ij} has a value of one. The values for ε_{ij} and σ_{ij} are the same as those used in the intramolecular non-bonded interactions. A potential cut-off of 17 Å is used to increase computational efficiency.

2.2.3 Molecule-Surface Interactions

The molecule-surface interaction is modeled using a modified Steele's potential. Steele's potential [**22**] is based on a Lennard-Jones 12-6 functional form and assumes that all of the carbon atoms in the basal plane (0001) of the graphite slab are in their equilibrium positions. From this starting position, it is possible to derive an expression for the potential energy interaction of any atom in the alkane molecule with the entire graphite surface.

$$U_{surf} = V_o(z) + \sum_{n>0} V_n(z) f_n(x,y) \qquad \textbf{2.11}$$

The terms in the sum converge quickly, so only V_1 and f_1 are used in the calculation of the potential energy. The forms for V_o, V_1, and f_1 are as follows:

$$V_o(z) = \frac{4\varepsilon\pi A^6}{a_s} \sum_{p=0}^{\infty} \left(\frac{2A^6}{5(z + p\Delta z)^{10}} - \frac{1}{(z + p\Delta z)^4} \right) \qquad \textbf{2.12}$$

$$V_1(z) = \frac{2\varepsilon\pi A^6}{a_s} \left[\frac{A^6}{30} \left(\frac{g_1}{2z} \right)^5 K_5(g_1 z) - 2 \left(\frac{g_1}{2z} \right)^2 K_2(g_1 z) \right] \qquad \textbf{2.13}$$

$$f_1(x,y) = -2 \left[\cos\left(\frac{4\pi x}{\sqrt{3}} \right) + \cos\left(\frac{2\pi x}{\sqrt{3}} - 2\pi y \right) + \cos\left(\frac{2\pi x}{\sqrt{3}} + 2\pi y \right) \right] \qquad \textbf{2.14}$$

where A is the value of σ for the alkane atoms and graphite surface normalized by the graphite lattice constant, a_s is related to the area of the graphite unit cell, Δz is the z-distance between graphite planes in the slab, K_i is the Bessel function of order i, and g_1 is the magnitude of the first reciprocal lattice vector. Values for a_s, Δz, g_1, and A for both carbon and hydrogen atoms are shown in Table **2-2**.

Table **2-2**: Potential Energy Parameters for Molecule-Surface Interactions

Parameter	Value
a_s	0.866
Δz	1.38
g_1	$4\pi/\sqrt{3}$
A_C	1.38
A_H	1.20

More recent research [**23**] has modified the corrugations in Steele's potential by adding an extra factor, s, to the expression for the potential energy, giving

$$U_{surf} = V_o(z) + sV_1(z) f_1(x,y) \qquad \textbf{2.15}$$

This research shows that an s-value of 1.0, the value in Steele's original potential, does not provide sufficient corrugation to match experimental desorption energies. A value of 1.5 is recommended.

The enhanced sampling techniques used in accelerated molecular dynamics reveal a flaw in Steele's potential that has heretofore not been discussed. Physically, as a molecule moves toward the graphite surface, it should initially experience an attractive force. As it moves closer than the preferred binding distance, it will experience a repulsive force. For the terms that depend exclusively on the z-distance of the atoms in the molecule from the surface (V_o and V_1), this is the case. V_o and V_1 become large positive numbers as the z-distance is decreased. However, the cosine functions in f_1 cause alternating positive and negative values. When the z-distance is close to the preferred binding distance, the expression for U_{surf} is dominated by the V_o term and remains consistent with physical reality. As the z-distance decreases, the V_1 term grows until it is comparable in magnitude to the V_o term. Then, the alternating positive and negative values of the f_1 term cause spurious potential energy minima to appear. An additional term must be added to Steele's potential to counteract this mathematical artifact.

$$U_{surf} = V_o(z) + s(1-\kappa)V_1(z) f_1(x,y) \qquad \textbf{2.16}$$

κ is defined as follows. At z-distances greater than 2.21 Å, κ has a value of zero, and the expression for the molecule-surface potential energy is given by Eq. **2.15**. At a z-distance of 2.09 Å, κ has a value of one, and the molecule-surface interaction is given exclusively by the V_o term in Steele's potential. As the z-distance decreases from 2.21 to 2.09 Å, κ increases linearly from 0 to 1, slowly and smoothly turning off the corrugations.

2.3 Constrained Dynamics - RATTLE

The time step in an MD simulation is limited by the fastest movement in the system. The time step must be smaller than the highest frequency motion. In the case of molecules, these motions include bond stretches and bond-angle bends. To allow for longer time steps, algorithms have been designed to constrain these high frequency motions to their equilibrium positions by the use of holonomic (position dependent) constraints. One such algorithm, RATTLE, was developed by Andersen in 1983 [**24**]. Along with constraining the positions of atoms in the high frequency motions, RATTLE also uses the derivatives of the holonomic constraints to constrain velocities of the atoms involved in the high frequency motions. Since velocities are included explicitly in the RATTLE algorithm, it is well suited to be used in simulations that utilize velocity rescaling as a method of temperature control.

In the simulations performed for this thesis, the three highest frequency modes were constrained using the RATTLE algorithm. These include the carbon-carbon bond stretches (1000 cm^{-1}), carbon-hydrogen bond stretches (3000 cm^{-1}), and hydrogen-

carbon-hydrogen angle bends (1400 cm^{-1}) [**25**]. By constraining these components of the alkane molecules to their equilibrium positions, it is possible to increase the time step of the simulations to 1.0 fs. The MD algorithm from Section 2.1 is modified to include the RATTLE algorithm in the following manner:

1. Positions are advanced one full time step according to Eq. **2.5**. Velocities are advanced one half time step according to Eq. **2.3**.
2. The bond length and bond angle position constraints are satisfied by iteration within the RATTLE algorithm.
3. Forces are calculated at the advanced time step (based on the positions calculated in step 1).
4. Velocities are advanced an additional half time step according to Eq. **2.3**.
5. The bond length and bond angle velocity constraints are satisfied by iteration within the RATTLE algorithm.

In this way, the simulation has advanced a full time step in both position and velocity, and all constraints have been satisfied.

2.4 Temperature Control

As implemented using the methods described in Section 2.1, an MD simulation is run at constant number of particles, volume, and energy. Since experiments are run at a fixed temperature, fixed pressure, or both, these variables must be controlled in a

simulation to allow for comparison between experimental results and simulation results. In the simulations described in this thesis, temperature control is implemented using the Berendsen thermostat [**26**]. This algorithm combines some of the physicality of a true canonical system through local temperature fluctuations with the ease of implementation that comes from a velocity rescaling method. With the Berendsen thermostat, the velocities of each atom are rescaled every time step according to the formula

$$\frac{v_{new}}{v_{old}} = \left[1 + \frac{1}{\tau}\left(\frac{T_{set}}{T} - 1\right)\right]^{0.5} \qquad \textbf{2.17}$$

where v_{new} is the rescaled velocity, v_{old} is the velocity before rescaling, T_{set} is the desired set point temperature, T is the instantaneous temperature, and τ is a coupling constant. The form of Eq. **2.17** has the effect of coupling the simulation system to an external heat bath. The value of τ controls the strength of the coupling: a smaller value of τ leads to a stronger coupling between the system and the external heat bath. Table **2-3** shows the values of the coupling constant for the simulations described in the remaining sections of this thesis.

Table **2-3**: Parameters for Berendsen Thermostat

Simulation Type	τ
Single Molecule	400.0
Layer	400.0
TPD	100.0

The coupling constant in the case of the TPD simulations is chosen slightly lower than in the single molecule and layer simulations because, while the temperature is continuously changing in the TPD simulations, the single molecule and layer simulations are fixed-temperature simulations.

2.5 Periodic Boundary Conditions

Periodic boundary conditions are implemented within the layer and TPD simulations. They allow a finite number of molecules to simulate a larger system more closely. A box of a given size is repeated infinitely in the chosen periodic directions. In practice, this is achieved by following the periodic images of a molecule. That is, when a molecule leaves the simulation box, its periodic image reappears on the opposite side of the simulation box [**27**]. This is shown schematically in Figure **2-1** where the central box is the simulation box and the lettered boxes are the repeated boxes in two directions.

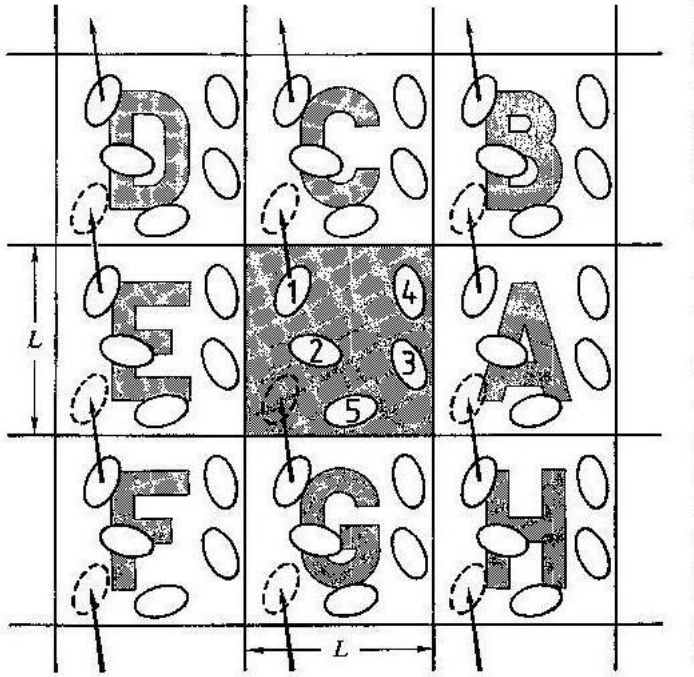

Figure **2-1**: Schematic of Periodic Boundary Conditions – Taken from [**27**]

In the surface simulations found herein, periodic boundary conditions are applied in the plane of the surface only. That is, the simulation box is periodic in x and y (the plane of the surface) but not in z.

2.6 Transition-State Theory

Rates of rare events and simulations of these events are based on transition-state theory (TST) [**28**]. The Van't Hoff-Arrhenius law [**29**] is the foundation of TST. It states

$$k = \nu \exp(-\beta E_b) \qquad \textbf{2.18}$$

where k is the rate of a process, ν is a prefactor, β is $(k_BT)^{-1}$, and E_b is the energy barrier for the process. Farkas [**30**], through the study of homogeneous nucleation, introduced the concept of rate of escape as a flux through a surface dividing "reactants" from "products." The two states involved in the rate may or may not be involved in a chemical reaction of any kind. As the theory was developed within the chemical kinetics field, these terms are often used to describe the beginning and ending states [**28**]. The defining equation in TST, developed by Eyring [**31**], is as follows

$$k_{TST} = \left(\frac{k_B T}{h}\right)\frac{Z^{\mp}}{Z_A}\exp\left(-\beta E_b\right) \qquad \textbf{2.19}$$

where k_{TST} is the rate as described by TST, h is Planck's constant, $Z^{\ddagger}$ is the partition function at the transition state between "reactants" and "products", and Z_A is the partition function at the "reactant" state A. Escape from the "reactant" state is governed by thermal fluctuations. Since the barriers to exit are often orders of magnitude larger than the magnitude of the thermal fluctuations [**28**], escape from the "reactant" state across the transition state to the "product" state is rare, thus the term "rare event." Implicit in the framework of TST are four key assumptions. These assumptions must hold in TST simulations for the simulation results to be valid. They are as follows:

1. A particle that has passed through the dividing surface at the transition state will always continue on to the "product" state. This assumption can be relaxed by the inclusion of a recrossing factor with a value less than one in Eq. **2.19**.
2. The "reactant" state is in thermal equilibrium. That is, the system spends enough time in the potential energy basin defining the "reactant" state to come to a thermal equilibrium before crossing the transition state dividing surface.

3. The "reactant" state is in thermal equilibrium with the state of the system at the transition state. That is, the system obtains a Boltzmann distribution of velocities at the transition state.
4. Classical mechanics applies to the system. More recently, this assumption has also been able to be relaxed due to advances in semi-classical quantum mechanics [**28**].

Generally, the TST rate can be described by the following equation

$$k_{TST} = \frac{1}{2}\frac{\iint \delta_{ij}\Theta_i \mid v_\perp \mid \exp\left(-\beta\left(K+V\right)\right)dxdp}{\iint \Theta_i \exp\left(-\beta\left(K+V\right)\right)dxdp} \qquad \textbf{2.20}$$

where k_{TST} is the TST rate of a process taking the system from state i to state j, δ_{ij} is the delta function at the transition-state hyperplane between states i and j, Θ_i equals 1 if the system is in state i and 0 otherwise to ensure that the integrals span the phase space from state i to its corresponding transition state, $v_\perp$ is the velocity orthogonal to the transition-state hyperplane, K is the kinetic energy of the system and V is the potential energy of the system. The integrals are calculated over the positions and momenta of all particles in the system [**32**].

In the case of alkane desorption, there are several processes that accompany the main desorption process. Alkane molecules have many degrees of freedom. In the current simulations, bond angles are allowed to bend, torsion angles are allowed to rotate, and the molecule is allowed to move in the plane of the surface. While these can be described as multiple energy minima in a rigorous description of the potential energy surface, the time scales on which these events occur are orders of magnitude smaller than

the time scale necessary for desorption to occur. It can thus be assumed that any molecule on the surface is at equilibrium regardless of the instantaneous bond angles, torsion angles, or position in the plane of the surface. This simplifies the TST description of desorption to a one-transition problem. The only transition of interest is that of desorption itself. This greatly simplifies the mathematical description of the flux of alkane molecules through the transition state dividing surface to [**2**]

$$k_{TST} = \frac{1}{2}\left(\frac{2k_B T}{\pi m}\right)^{0.5} \frac{\int_R \delta[F(R)]\, e^{-V(R)\beta} dR}{\int_R e^{-V(R)\beta} dR} \qquad \textbf{2.21}$$

where k_{TST} is the TST desorption rate, m is the mass of the alkane molecule, δ is the delta function, F(R) is a function that is equal to zero at the transition state, V(R) is the potential energy of the system, and the integrals span the entire range of phase space from the graphite surface to the transition state dividing surface. Since alkane adsorption is not an activated process, there is no clear transition state for desorption between the "reactant" state (on the surface) and the "product" state (complete desorption). Instead, the transition state surface is placed where the number of recrossings is minimized [**28**]. That is, the transition state is defined at the perpendicular distance from the graphite surface where all atoms of the alkane molecule would have a negligible interaction with the surface even if the alkane molecule was aligned with its long axis parallel to the surface normal. This ensures that the alkane molecule will have negligible interaction with the surface regardless of its orientation.

Applying Eq. **2.21** to a conventional MD simulation is fairly straightforward. The integrals in Eq. **2.21** become sums of time steps according to the following equation

$$k_{TST} = \frac{1}{2}\left(\frac{2k_B T}{\pi m}\right)^{0.5} \frac{N_{TS}}{N_{TOTAL}} \qquad \textbf{2.22}$$

where N_{TS} is the number of time steps at the transition state and N_{TOTAL} is the total number of time steps in the simulation. However, due to the large energy barrier to desorption, few trajectories reach the transition state in a conventional MD simulation. Therefore, the numerator in Eq. **2.22** cannot be sampled and evaluated accurately. Strategies for increased transition state sampling are discussed in Section 2.7.

2.7 Acceleration Schemes

As discussed in the Section 2.6, sampling regions near the transition state in conventional MD simulations can be exceedingly difficult or nearly impossible. Recent developments in accelerated MD methods have been focused on increasing the rate of rare-event transitions while preserving their relative rates. Grimmelman et al., in studying the desorption of xenon from a platinum surface, proposed a method that adds a "compensating potential" to the actual potential energy surface [**1**]. This compensating potential fills in the potential energy well along a chosen reaction coordinate and allows desorption to occur more readily. A related method is hyperdynamics, developed by Voter [**3**]. In hyperdynamics, the MD simulation is run on a modified potential energy surface where the process of interest occurs more readily. The modified potential energy surface is related to the actual potential surface by a boost potential ΔV,

$$V^* = V + \Delta V \qquad \textbf{2.23}$$

where V^* is the modified potential energy surface and V is the actual potential energy surface. The formulation for the rate on the modified potential energy surface becomes

$$k_{TST}^{b} = \frac{1}{2}\frac{\iint \delta_{ij}\Theta_i \mid v_{\perp} \mid \exp\left(-\beta\left(K+V\right)\right)dxdp}{\iint \Theta_i \exp\left(-\beta\left(K+V+\Delta V\right)\right)dxdp} \qquad \textbf{2.24}$$

where k^b is the rate on the modified potential energy surface. The rate on the modified potential energy surface can be related to the rate on the actual potential energy surface by combining Eq. **2.20** and Eq. **2.24** and producing

$$k_{TST} = k_{TST}^{b}\frac{1}{\left\langle \exp\left(\beta\Delta V\right)\right\rangle_b} \qquad \textbf{2.25}$$

where $\langle\ldots\rangle_b$ is an ensemble average evaluated on the modified potential energy surface. Additionally, the average time to escape a potential minimum can be written as the inverse of the rate of escape. This gives a physical time which is an ensemble average and can be described by the equation [**3**]

$$t = t_b\left\langle \exp\left(\beta\Delta V\right)\right\rangle_b \qquad \textbf{2.26}$$

where t_b is the time elapsed on the modified potential energy surface (simulation time) and t is the corresponding time on the actual potential energy surface (physical time).

The form of ΔV is chosen to enhance escape from local minima while leaving the potential energy surface unchanged at the transition states. This preserves relative rates of escape and the dynamics of the system. However, it means that transition states must be known a priori or detected through the course of the simulation. In Voter's hyperdynamics [**3**] this is accomplished by calculating the eigenvalues of the Hessian matrix (the matrix of second derivative components of position) and finding a negative

eigenvalue that corresponds to a transition state. While this method will rigorously find the transition states in a system, it is computationally inefficient and can be used only for small system sizes. To combat this computational problem, Miron and Fichthorn developed a method that uses a physical description of the transition state to control the boost function [**4**]. Since the positions of the atoms in the system are already known and do not need to be calculated, very little computational overhead is introduced with this method when compared to the large computational overhead of finding the eigenvalues of the Hessian matrix.

In the same manner as the MD simulations discussed in Section 2.6, Eq. **2.24** can be simplified for the case of desorption. This produces an expression for the TST rate constant based on a weighting function W(R)

$$k_{TST} = \frac{1}{2}\left(\frac{2k_B T}{\pi m}\right)^{0.5} \frac{\int_R \delta[F(R)] W(R)\, e^{-V(R)\beta} / W(R) dR}{\int_R W(R)\, e^{-V(R)\beta} / W(R) dR} \qquad \textbf{2.27}$$

The weighting function is defined as

$$W(R) = \exp\left(\frac{V(R) - V^*(R)}{k_B T}\right) \qquad \textbf{2.28}$$

Simplifying Eq. **2.27**, an expression for the TST rate constant containing averages on the modified potential energy surface is obtained:

$$k_{TST} = \frac{1}{2}\left(\frac{2k_B T}{\pi m}\right)^{0.5} \frac{\langle \delta[F(R)]/W \rangle_b}{\langle 1/W \rangle_b} \qquad \textbf{2.29}$$

where $\langle \ldots \rangle_b$ indicates a canonical average evaluated on the modified potential energy surface.

In the case of thermal desorption, the physical description of the transition state is straightforward. Once an alkane molecule has reached a certain perpendicular distance from the graphite surface, the interaction between the alkane molecule and the graphite surface is negligible. Thus, this z-distance of the center-of-mass of the alkane molecule provides a suitable physical description of the transition state. For computational reasons, it is beneficial to model the transition-state hyperplane as a thin box with a width *b*. The expression for the rate constant must be normalized by this width and becomes

$$k_{TST} = \frac{1}{2}\left(\frac{2k_B T}{\pi m}\right)^{0.5} \frac{1}{b} \frac{\langle \delta[F(R)/W] \rangle_b}{\langle 1/W \rangle_b} \qquad \textbf{2.30}$$

Applying Eq. **2.30** to an MD simulation on the modified potential energy surface produces an expression much like Eq. **2.22**. Here, instead of simulation time (i.e. N) in the numerator and denominator, the rate constant depends on physical times (i.e. W).

$$k_{TST} = \frac{1}{2}\left(\frac{2k_B T}{\pi m}\right)^{0.5} \frac{1}{b} \frac{\sum_{At\ TS} 1/W}{\sum_{TOTAL} 1/W} \qquad \textbf{2.31}$$

where the numerator is the sum of 1/W in the box defining the transition state and the denominator is the sum of 1/W over the entire simulation.

Specific forms of the modified potential energy surface depend on the physical characteristics of the simulation and are different for single molecules versus layers, for example. Each form will be discussed in detail in the appropriate section.

2.8 Simulation Measures

A number of measures are monitored to ensure that the results obtained from accelerated simulations are physically meaningful. These values are calculated for conventional MD simulations where no desorption events occur. Then, they are compared to accelerated simulations at corresponding temperatures and coverages to ensure that the acceleration scheme is not unfairly biasing the simulation in any way. This ensures that the molecular environment of the accelerated system is the same as that for the unaccelerated system.

2.8.1 Energy Histogram

Energy histograms are created by sampling the potential energy of the total system. In the case of the conventional MD simulations, each sampled energy is weighted equally. Therefore, the probability that the energy of the system falls between an energy E and an energy E + ΔE is given by

$$P(E+\Delta E) = \frac{N(E+\Delta E)}{N_{TOTAL}\Delta E} \qquad \textbf{2.32}$$

where N(E+ΔE) is the number of sampled steps that fall between E and E+ΔE and N_{TOTAL} is the total number of sampled steps. In the current simulations, the widths of the energy bins are constant across the entire energy range.

In the case of the accelerated simulation, each sampled energy is weighted according to the amount of physical time that the system spends at that energy. Recall from Section 2.7 that the physical time is related to the simulation time by the expression,

$$t = t_b \left\langle \exp\left(\beta \Delta V\right) \right\rangle_b \qquad \textbf{2.33}$$

and that the weighting factor is defined as

$$W(R) = \exp\left(\frac{V(R) - V^*(R)}{k_B T} \right) \qquad \textbf{2.34}$$

The probability expression for simulations on the modified potential energy surface then becomes

$$P\left(E + \Delta E\right) = \frac{\sum \frac{1}{W\left(E + \Delta E\right)}}{\Delta E \sum \frac{1}{W}} \qquad \textbf{2.35}$$

where W(E+ΔE) are the weighting factors for the sampled steps that fall between E and E+ΔE and W are the weighting factors for all of the sampled steps.

The energy histograms for the unaccelerated and accelerated systems are plotted on the same set of axes. Systems that exhibit proper acceleration will have energy histograms that overlap, meaning that the same range of energies is being sampled in both the accelerated and unaccelerated system.

2.8.2 Radial Distribution Function

The radial distribution function (RDF) is a measure of the ratio between the average number of particles found in a spherical shell at a distance r with a thickness of dr and the average number of particles found in the same spherical shell in an ideal gas with the same density. In the case of the simulations performed here, the RDF is a two-dimensional measure based on the center-of-mass of the alkane molecules. That is, the

radial distribution is calculated based on only the x-y distance between the center-of-mass of each alkane molecule and compared to a surface coverage based on an even distribution of molecules on the surface. As with the energy histograms, the RDF values must be weighted by the proper time factor, W, from Eq. **2.34** in the accelerated systems. Unweighted RDF from conventional MD simulations are compared to weighted RDF from the accelerated systems. In simulations where the structure of the layer is preserved in the accelerated system, the peaks in the RDF of the accelerated system will correspond in height and position to the peaks in the RDF of the conventional MD simulation.

2.8.3 Roll Angle Distribution

The roll angle is the angle that the plane of the long axis of the alkane molecule makes with the plane of the graphite surface. In the lowest possible energy state, alkane molecules lie with the backbones parallel to the graphite surface [**15**], a roll angle of 0 or 180 degrees. As the temperature is increased, molecules obtain the kinetic energy needed to roll along their long axis. This increases the contact that a molecule has with neighboring molecules and decreases the interaction it has with the surface. By looking at the roll-angle distribution, one can examine the balance between intermolecular forces and molecule-surface forces. Comparing this measure between a conventional MD simulation and an accelerated simulation helps to ensure that this force balance is preserved in spite of the acceleration.

2.8.4 Molecular Conformations

Conformational changes within the alkane molecule can also be monitored. Each alkane molecule contains N-3 carbon backbone torsion angles where N is the number of carbon atoms in the alkane molecule. Since the alkane molecules are symmetric, torsion angles the same distance from each end are also symmetric. Torsion angles are defined to be in the gauche conformation if the angle value in the simulation is less than $-\pi/3$ or greater than $\pi/3$. If any of the torsion angles are in the gauche conformation, the molecule is considered to be in the gauche conformation. It is also possible to determine which torsion angle is in the gauche conformation when a conformation change occurs. These conformational changes will be discussed in detail as they pertain to the single molecule simulations in **3.3**.

Chapter 3

Single Molecule Simulations

Although single molecule simulations provide a simplistic approach to the desorption problem, they still offer insight into the behavior of alkane molecules on a graphite surface. In TPD experiments, it is often assumed that the desorption energy and prefactor are independent of coverage. If this is truly the case, the zero-coverage (single molecule limit) simulations performed in this chapter should explain the characteristics of the experimental data. However, as simulations from Chapter 5 show, this is not the case.

A single alkane molecule is placed on an infinite graphite surface and allowed to desorb. The alkane molecules studied range from pentane (C_5H_{12}) to hexadecane ($C_{16}H_{34}$). This allows examination of the effect of chain length on desorption energetics at the zero-coverage limit.

3.1 Acceleration Method

Two different forms of the boost potential ΔV (as defined in Eq. **2.23**) are used in the single molecule case. Each will be described in detail along with comparing the relative merits of each.

3.1.1 Temperature Acceleration

Escape from local minima on the potential energy surface is accomplished via local thermal fluctuations. At experimentally relevant temperatures, these fluctuations are too small to allow for escape on MD time scales. However, as the temperature is increased, the fluctuations increase as well. At temperatures higher than those used in desorption experiments, alkane desorption does occur on MD time scales. This idea is the basis for the form of ΔV. The simulation is run at a high temperature sT where desorption occurs on MD time scales [**7**]. Then, the results are scaled back to an experimentally relevant temperature, T. This is equivalent to running the simulation on a modified potential energy surface that is the actual potential energy surface divided by the temperature scaling factor s

$$V^* = \frac{V}{s} \qquad \textbf{3.1}$$

where *s* is greater than one. Using Eq. **2.28**, one can obtain an expression for the weighting factor, *W*

$$W(R) = \exp\left[\left(\frac{s-1}{s}\right)\frac{V(R)}{k_B T}\right] \qquad \textbf{3.2}$$

One advantage of using this formulation for the modified potential energy surface is the increased efficiency in running accelerated simulations. The simulation can be run at one higher temperature sT and scaled back to multiple lower temperatures to obtain a full Arrhenius plot from one run.

The high temperature sT must be chosen carefully to preserve the relevant physics of the system, while still allowing desorption to occur. If the chosen high temperature is

too high, extreme acceleration results. The energies (and molecular configurations) sampled by the accelerated simulation will be different than the energies sampled in the conventional MD simulation. This extreme acceleration is shown in Figure **3-1**.

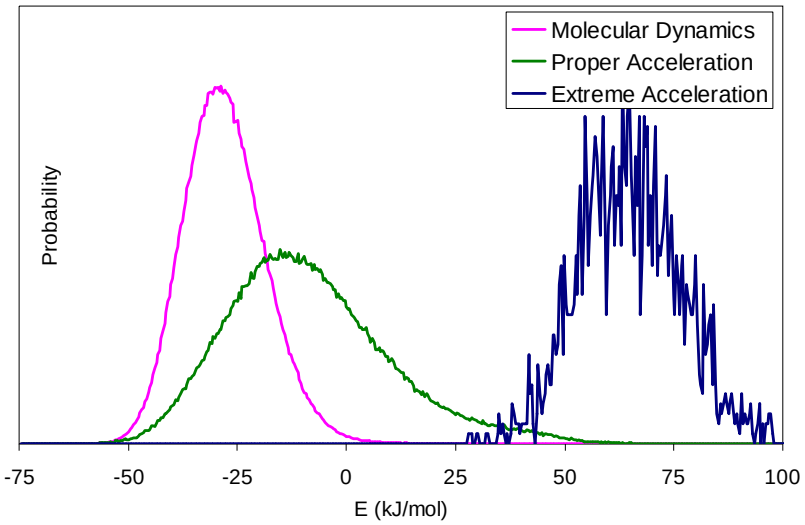

Figure **3-1**: Sample Energy Histogram – Proper and Extreme Acceleration

If the chosen high temperature is too low, no desorption events will occur on MD time scales. Proper acceleration involves a temperature that is high enough for desorption to occur, while ensuring that the lowest energy configurations characteristic of desorption at the experimental temperature are still sampled. This balance is verified by examining energy histograms that were collected as discussed in Section **2.8.1**. One such histogram for the desorption of pentane from the graphite surface is shown in Figure **3-2**.

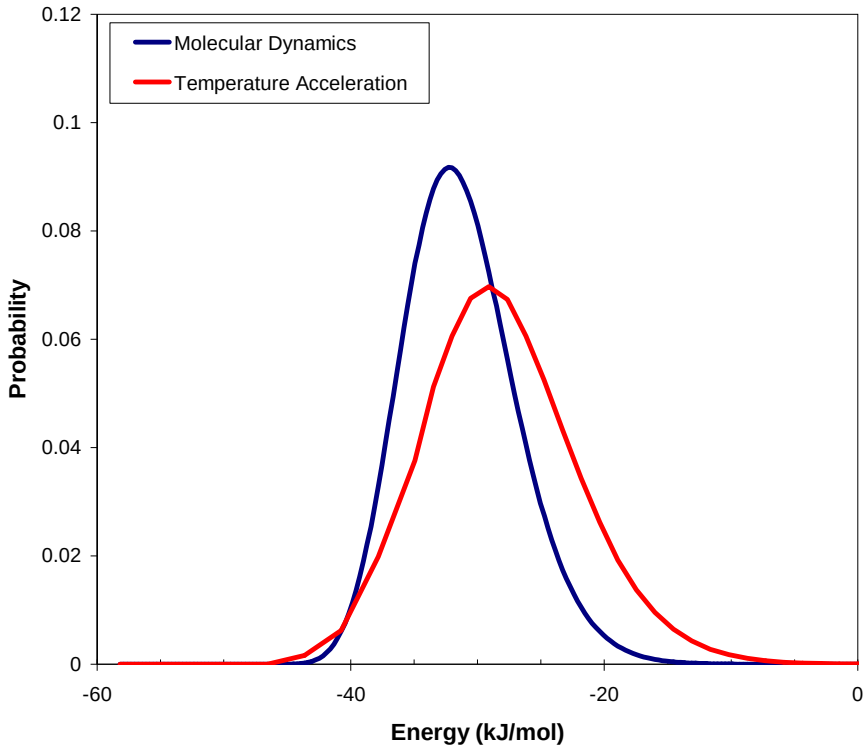

Figure **3-2**: Energy Histogram – Pentane, 165 K

As can be seen in the figure, the lowest energies (-45.0 kJ/mol) are sampled in both the conventional MD simulations and the temperature-accelerated simulations. The temperature-accelerated simulations also increase the energy range that is sampled to include higher energy configurations corresponding to molecules desorbed from the graphite surface. High temperature values for each molecule along with the corresponding *s* values can be found in Table **3-1**.

Table **3-1**: High Temperature Values for Temperature Acceleration

Number of Carbons	sT	Low s	High s
5	500	2.78	3.85
6	600	3.00	4.00
7	650	2.83	3.61
8	700	2.50	3.50
10	800	2.67	3.64
12	1000	2.86	4.00
14	1100	2.75	3.67
16	1150	2.88	3.83

Since the temperature acceleration method is highly efficient and allows for multiple temperature points to be obtained from one simulation, a majority of the results in this section were obtained from temperature accelerated simulations.

3.1.2 Compensating Potential

For comparison, we also used a compensating potential boost function, similar to that used by Grimmelman et al. [**1**]. The compensating function serves to decrease the interaction between the alkane molecule and graphite surface. The original form of the weighting function resulting from this change is

$$W(R) = \exp\left[(1-\alpha)\frac{U_s}{k_B T}\right] \qquad \textbf{3.3}$$

where α is an empirical parameter between zero and one that controls the extent of acceleration and U_s is the molecule-surface potential energy function, as given by Eq. **2.16**.

However, we found when only the molecule-surface interaction was decreased to allow desorption on MD timescales, conformational changes within the molecule occurred on the same time scale as desorption events. Thus, conformational changes within the alkane molecules were not sampled properly on the modified potential energy surface. To preserve the relative timescales of the two processes (desorption and conformational changes), the torsion interactions were also decreased by a factor of α. This results in a new weighting function that includes both the molecule-surface interaction and the torsion interactions

$$W(R) = \exp\left[(1-\alpha)\frac{(U_s + U_t)}{k_B T}\right] \qquad \textbf{3.4}$$

where U_t is the torsional component of the potential energy given by Eq. **2.8**. As with the temperature acceleration, it is possible to create a case of extreme acceleration if the value of α is too small. The value of α used in the compensating potential simulations was 0.3.

3.1.3 Acceleration Method Comparison

In both cases, the simulations were run as follows. The alkane molecule was placed near the preferred binding distance from the surface with random coordinates in the plane of the surface. It was then rotated to a random angle in the plane of the surface. The simulation was equilibrated for 5 picoseconds, and then the averages in Eq. **2.30** were accumulated. The velocity Verlet algorithm with RATTLE, as described in Section **2.3**, was used to advance time in the simulation. Once the molecule desorbed completely,

it was placed back on the surface at a different orientation and re-equilibrated. Rate constants were calculated for eleven different experimentally relevant temperatures [**5**]. The results were plotted on an Arrhenius plot, assuming that the desorption can be described by the form given by Eq. **1.1**. The conformation of each molecule was examined closely through multiple measures. The fraction of time that a molecule spent in the trans conformation (no torsion angles in a gauche conformation, as defined in Section **2.8.4**) along with the fraction of time that each individual torsion angle spent in the gauche conformation were monitored to correlate conformational changes within the molecule to experimental quantities.

To compare the performance of the two different acceleration schemes, Arrhenius plots for both temperature acceleration and compensating potential were calculated. As can be seen in Figure **3-3**, the rates at each temperature are within the error bars.

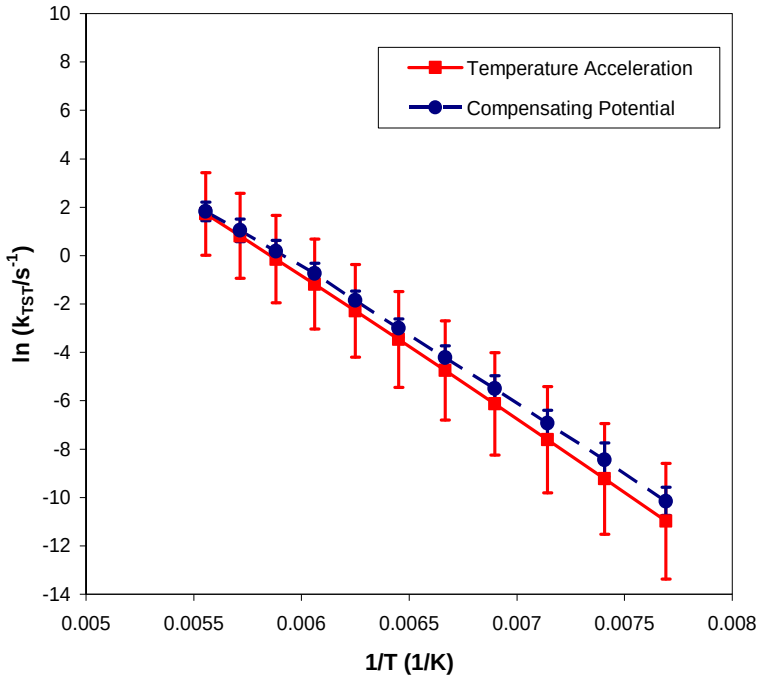

Figure **3-3**: Arrhenius Plots – Temperature Acceleration and Compensating Potential

Thus, for the single molecule case, the two methods are statistically equivalent. Due to the increased efficiency of the temperature acceleration method as discussed above, that is the method that was used for simulations producing the balance of the results in this section. However, the compensating method became the basis for the acceleration schemes in the fixed coverage case.

3.2 Arrhenius Plots – Variable Chain Length

Arrhenius plots were obtained for single alkane molecules ranging in length from pentane (C_5H_{12}) to hexadecane ($C_{16}H_{34}$). As shown in Figure **3-4**, they are linear in the

temperature range studied, corresponding to an experimentally relevant temperature range for desorption for each molecule.

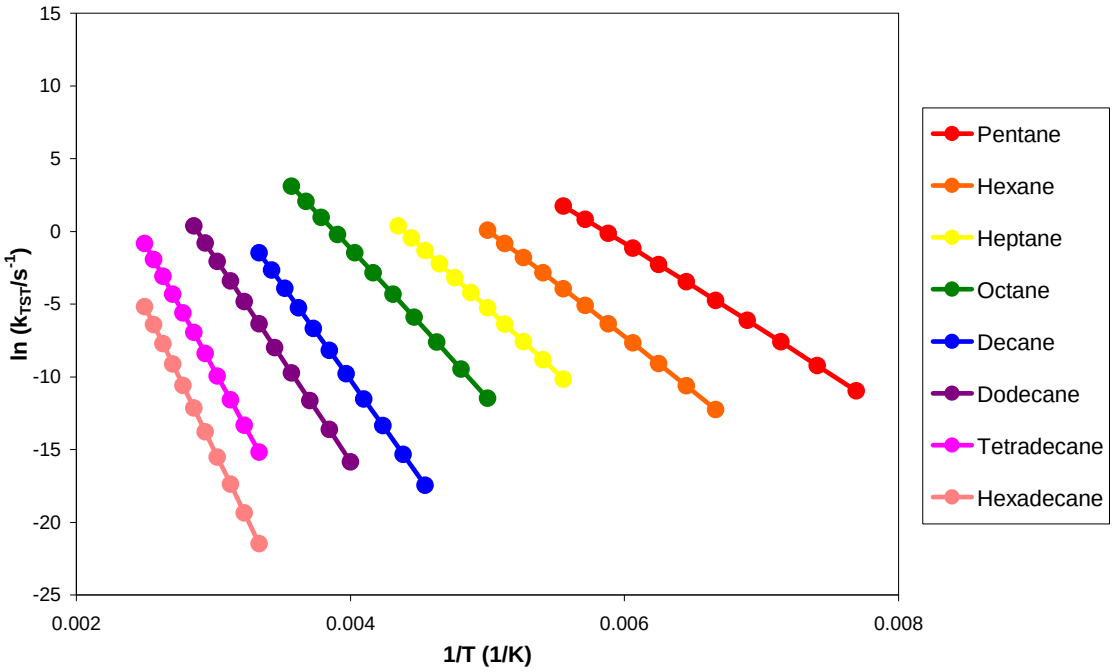

Figure **3-4**: Arrhenius Plots – Variable Chain Length

Analysis of the Arrhenius plots was based on Eq. **1.1**, and both desorption energies (E_d) and prefactors (ν) were obtained for each molecule. Results are summarized in Table **3-2**.

Table **3-2**: Simulated Desorption Energies and Prefactors

Number of Carbon Atoms	E_D (kJ/mol)	$Log_{10}(\nu/s^{-1})$	E_D all-trans (kJ/mol)
5	49 ± 2	15.1 ± 0.7	53.4
6	62 ± 2	16.1 ± 0.7	64.0
7	73 ± 3	16.7 ± 0.7	73.6
8	84 ± 2	17.1 ± 0.5	85.5
10	108 ± 4	18.3 ± 0.8	110.2
12	116 ± 4	17.7 ± 0.6	122.2
14	142 ± 5	18.3 ± 0.7	146.5
16	163.± 5	19.0 ± 0.7	166.2

Also included in Table **3-2** are all-trans binding energies for each molecule. These energies were obtained using the steepest descent method. The molecule was placed in an all-trans conformation at a height above the surface greater than the preferred binding distance. Then, the molecule was allowed to move at 0 K (due only to the forces caused by the potential energy) until a local minimum was reached. Multiple initial positions in the plane of the surface were attempted, and the lowest energy configuration observed was defined as the all-trans binding energy. As can be seen in Table **3-2**, the all-trans binding energy is lower than the desorption energy of the molecule, as calculated by TST. This can be explained by the multiple conformations and configurations that the alkane molecule can take on the surface. Pentane, the shortest molecule studied in this thesis, contains two equivalent carbon backbone torsion angles that can be found in the trans or gauche conformation. As the length of the molecule increases, the number of carbon backbone angles also increases, thereby increasing the number of possible configurations. In addition to possible trans-gauche conformational changes, there are also multiple local energy minimum configurations with the molecule in the all-trans configuration. As can be seen in Figure **3-5**, the lowest energy

configuration of the pentane molecule has a carbon backbone that zig-zags across the hexagons that define the basal plane surface.

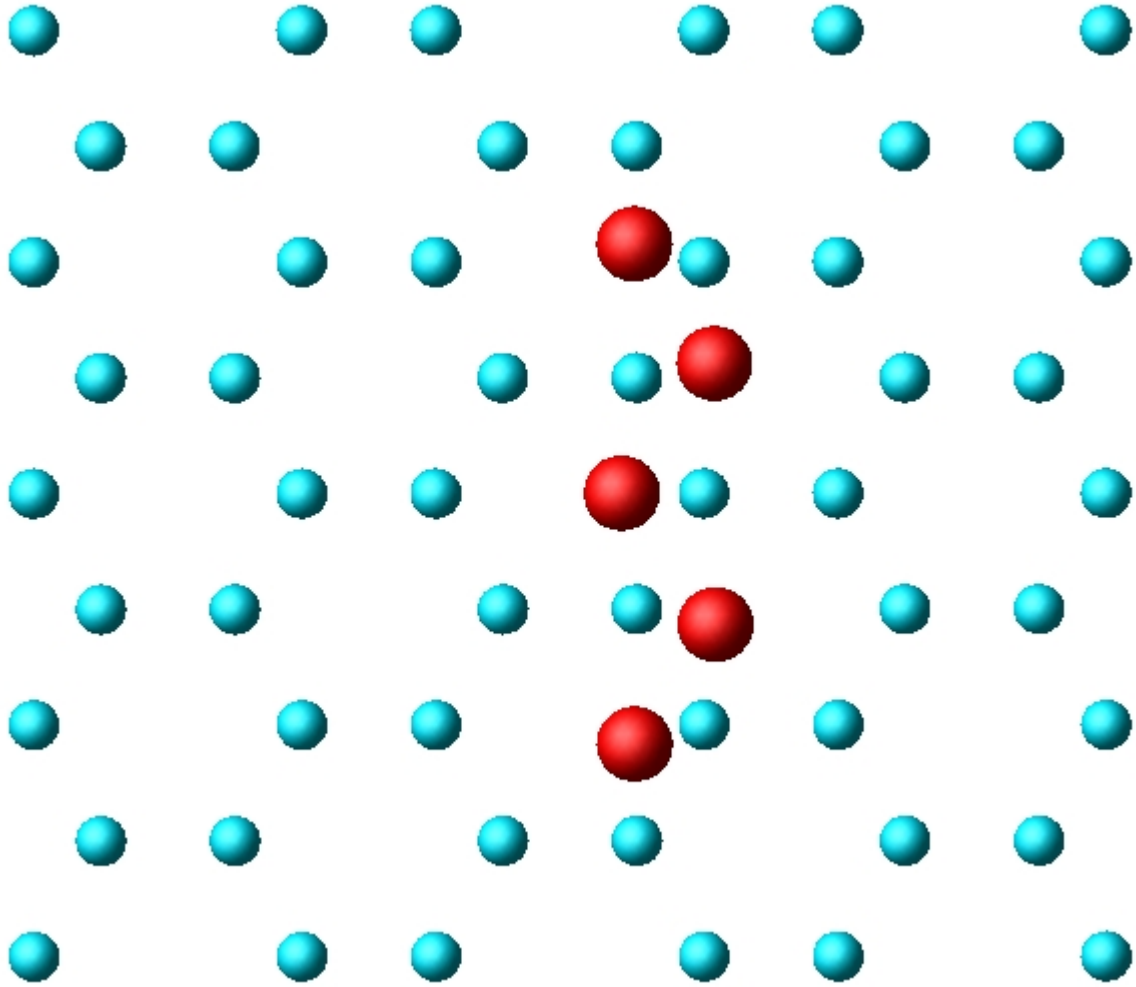

Figure **3-5**: Minimum Energy Configuration for Pentane (Hydrogen Atoms Omitted for Clarity)

In Figure **3-6**, the pentane molecule is still in the all-trans configuration. However, there is some overlap with carbon atoms in the graphite surface. As would be expected, this configuration has a higher energy than the configuration shown in Figure **3-5**. It is,

however, lower in energy than the configurations that contain one gauche backbone angle.

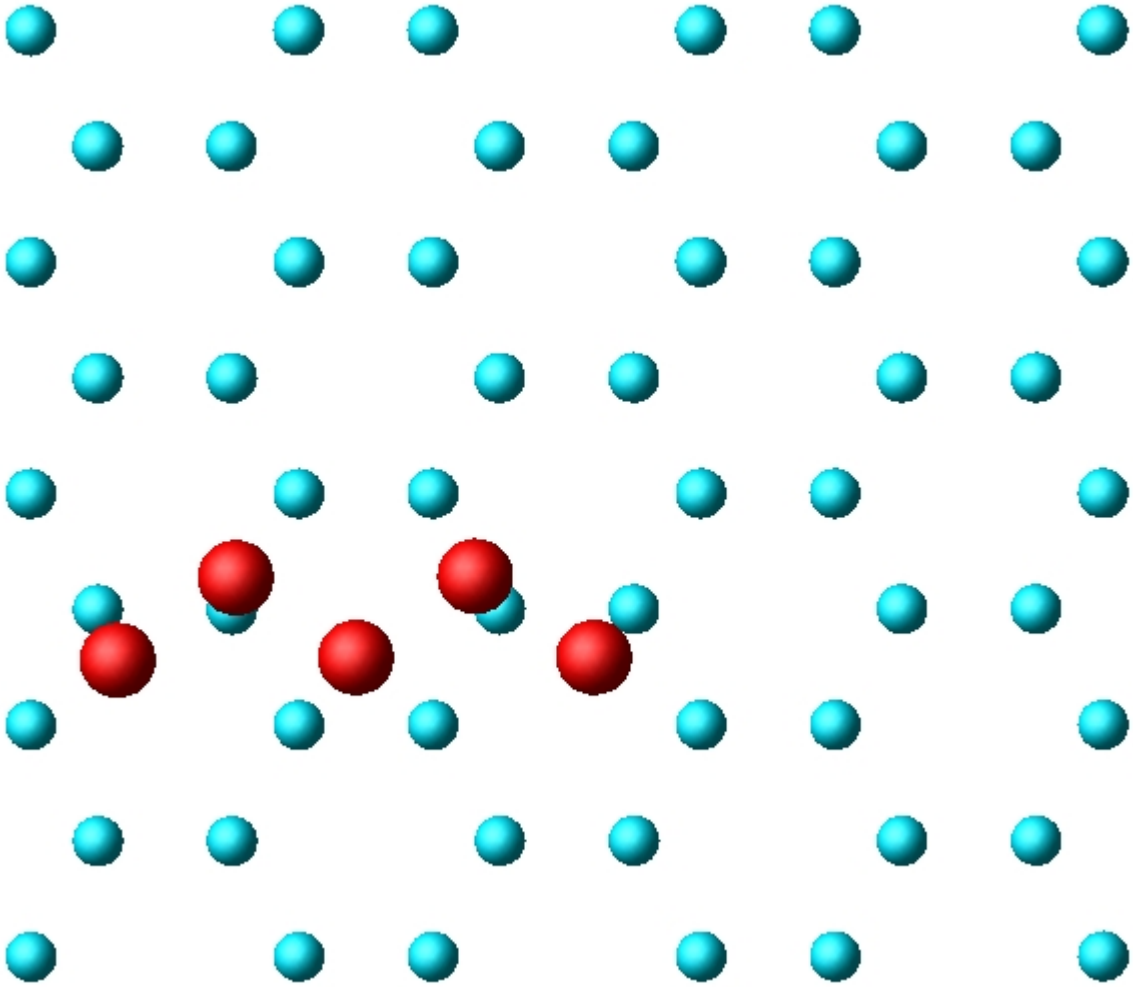

Figure **3-6**: Local Energy Minimum Configuration for Pentane (Hydrogen Atoms Omitted for Clarity)

Another notable aspect of the all-trans binding configurations is the effect that chain length has on the registry with the graphite surface. As mentioned above, there is a difference in length between the carbon-carbon distance in the alkane backbone and the carbon-carbon distance in the graphite hexagons. For short molecules such as pentane

(shown in Figure **3-5**), the molecule spans only a few graphite hexagons and can achieve registry with the graphite surface. In contrast, long molecules such as hexadecane span many more graphite hexagons. As more hexagons are spanned, the difference in carbon-carbon distance between the alkane molecule and the graphite surface is accentuated. Thus, as can be seen in Figure **3-7**, even though the carbon atoms at the center of the molecule are aligned with the graphite surface, the carbon atoms at the ends of the molecule cannot achieve registry.

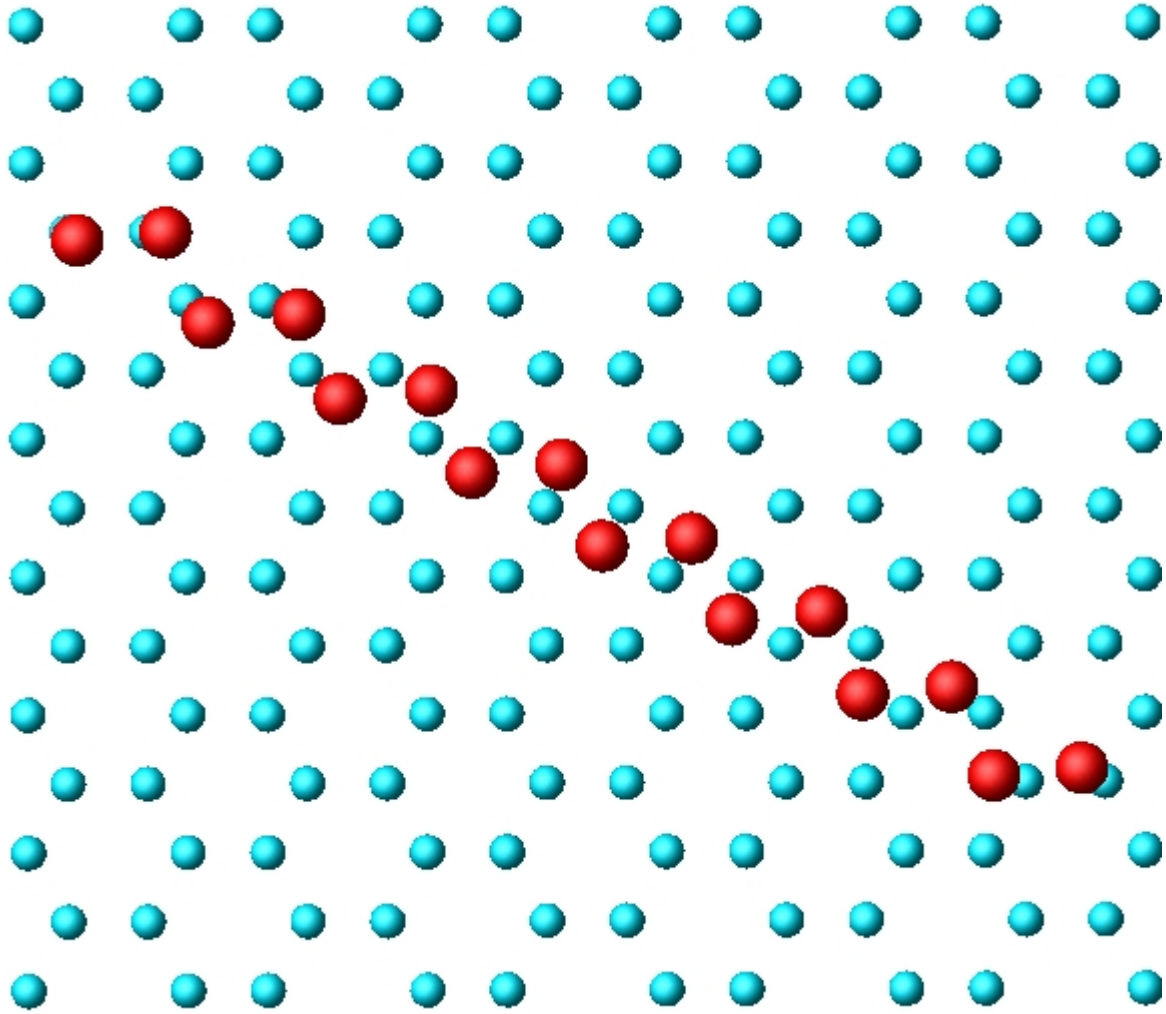

Figure **3-7**: Minimum Energy Configuration for Hexadecane (Hydrogen Atoms Omitted for Clarity)

The desorption energies obtained from the Arrhenius plots are compared to experimental desorption energies in Figure **3-8**. Here, the desorption energies for the short and mid-length alkanes compare favorably to experimental values from Tait et al. [**10**] and Paserba and Gellman[**5**].

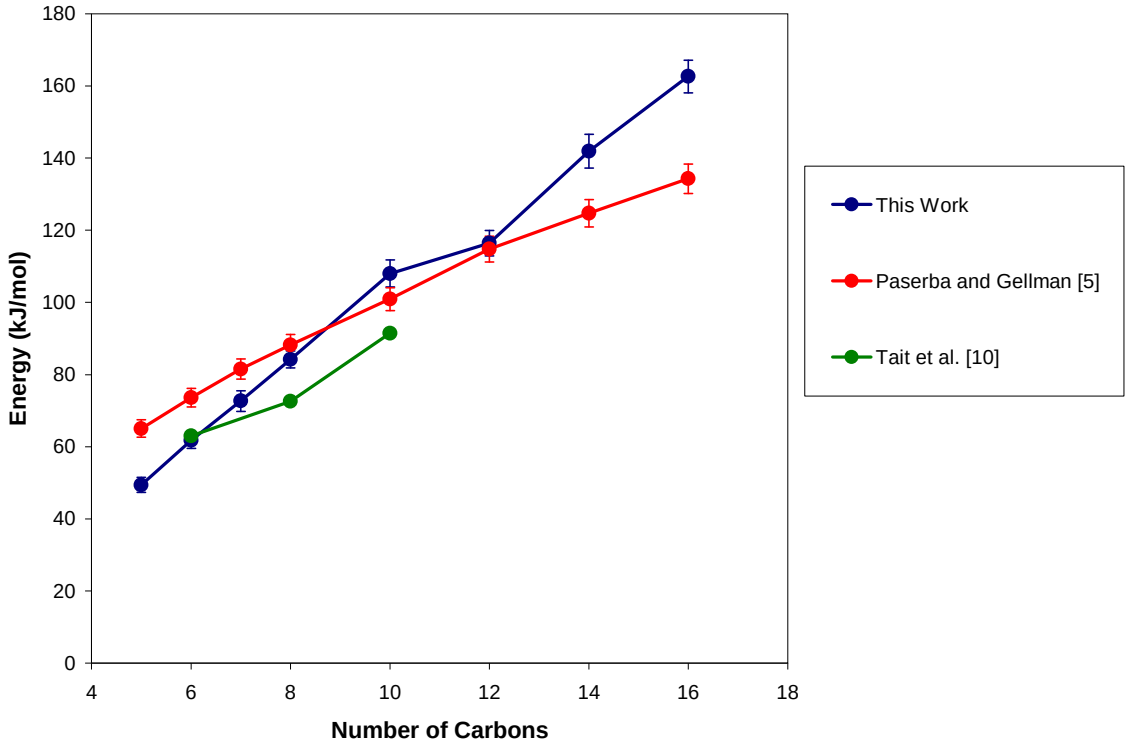

Figure **3-8**: Desorption Energy Comparison – Simulated and Experimental

The TST simulations tend to overestimate the desorption energy for the longer alkane molecules (tetradecane and hexadecane). This difference may result from the coverage difference between these single molecule simulations and the finite coverage experiments. As was shown in the layer and TPD simulations, intermolecular interactions are very important. These interactions were neglected in the single molecule simulations. As the longer molecules are examined, there are more interaction sites available, and the effect of neglecting them would be magnified.

As has been discussed in previous sections, there has been considerable disagreement in the literature regarding values of the prefactor and its functionality with alkane chain length. Figure **3-9** shows the values of the prefactor derived from the TST

simulations compared to those from the experiments of Tait et al. [**10**] and Paserba and Gellman [**5**].

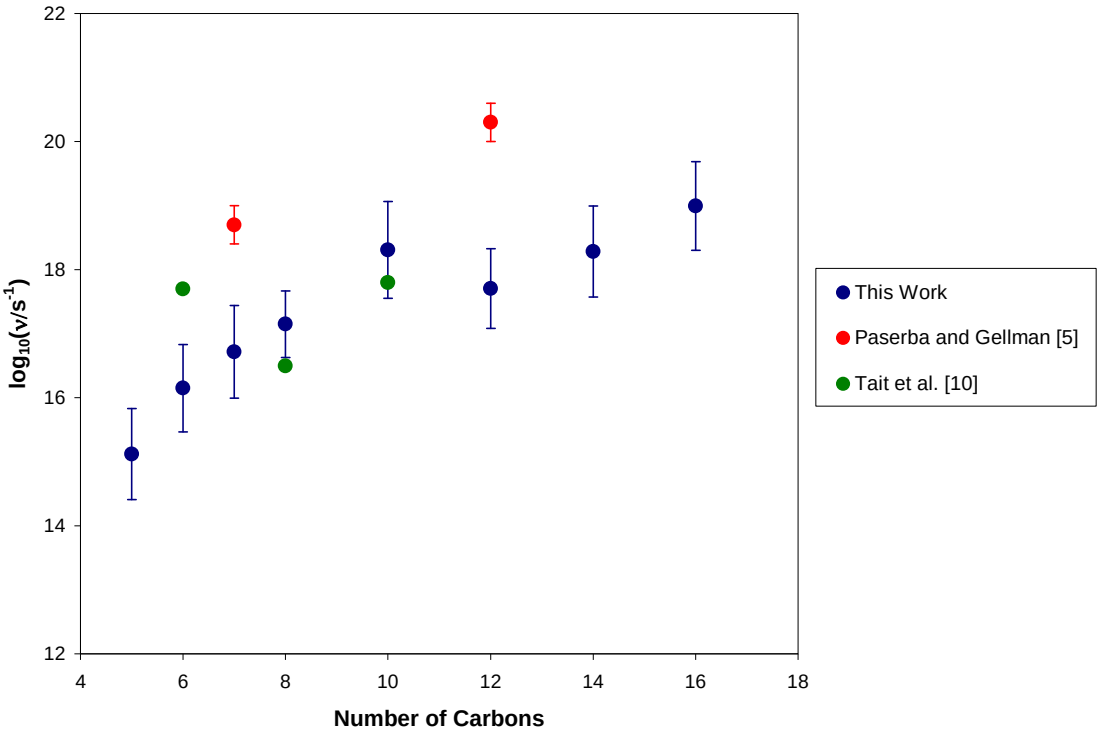

Figure **3-9**: Prefactor Comparison – Simulated and Experimental

Prefactors from the simulations for octane and decane are in good agreement with those from Tait et al. [**10**]. Other experimental prefactors (hexane, heptane, and dodecane) are underestimated by the simulation results. However, the difference in the simulated values and the experimental values is on the same order as the discrepancies between the two sets of experimental values. Again, it is important to note that the simulation results from this section are at the single molecule limit while the experimental results are at a finite coverage. Since the prefactor is related to entropy change on desorption (described in Section 3.3), the distinction in coverage differences can be of even more importance.

We note that the prefactor increases with increasing chain length for chains up to decane. Then, the prefactor levels off to a constant value of about $10^{18.3}$. We examine the role of conformational changes in the desorption process to explain the functionality of prefactor to chain length.

3.3 Role of Entropy in Prefactor

The prefactor in the Arrhenius expression for desorption is a measure of the entropy change on desorption. Mathematically, this can be written as

$$\nu = \frac{k_B T}{h} e^{\Delta S / k_B} \qquad \textbf{3.5}$$

where h is Planck's constant and ΔS is the difference between the entropy at the transition state (free gas molecule) and the entropy of the molecule on the surface (adsorbed molecule). The prefactor can also be expressed in terms of a ratio of partition functions at the transition state and on the graphite surface

$$\nu = \frac{k_B T}{h} \frac{Q^{\ddagger}}{Q} \qquad \textbf{3.6}$$

where $Q^{\ddagger}$ is the partition function of the alkane molecule at the transition state and Q is the partition state of the molecule on the graphite surface. Each partition function can be written as the product of individual partition functions for various degrees of freedom in the system

$$Q = q_t q_r q_v q_i q_e \qquad \textbf{3.7}$$

where q_t is the rigid-body translational partition function, q_r is the rigid-body rotational partition function, q_v is the vibrational partition function, q_i is the partition function for internal rotations, and q_e is the electronic partition function. Both at the transition state and on the graphite surface, the electronic partition function is the same, so it can be neglected in the prefactor analysis. Taking each of the rest of the components individually, it is possible to estimate their contribution to both the transition state partition function and the adsorbed molecule partition function.

At the transition state, one of the three rigid-body translational degrees of freedom becomes the motion of the alkane molecule over the transition state [**33**]. The remaining two rigid-body translational degrees of freedom are completely free. Alkane molecules move without barrier across the graphite surface at desorption temperatures. As a result, translational degrees of freedom in those directions are completely free. Translational motion in the third direction (into the surface) is completely restricted.

There are three rigid-body rotations that an alkane molecule can undergo. It can roll along its long axis (log-roll rotation), rotate in the plane of the surface (helicopter rotation), or rotate perpendicular to the plane of the surface (cartwheel rotation). At the transition state, all of these motions are completely free. However, they are affected in different ways at the surface. The cartwheel rotation is almost completely restricted at the surface due to the presence of the surface and the inability of the alkane molecule to rotate through it. The log-roll rotation is fairly free at the surface. As will be shown in Section **5.2** (variable coverage simulations), pentane molecules prefer to lie flat with the carbon backbone parallel to the surface. However, the entire range of log-roll angles is sampled with some probability (see Figure **5-3**). The helicopter rotation is an

intermediate rotation. The energy necessary to rotate the alkane molecule in the plane of the surface will depend on the number of carbon atoms in the molecule and will increase as the molecular length increases. As a result, the amount of entropy gained when the molecule goes from a bound state on the surface to a free gas at the transition state will also increase with increasing chain length. Tait et al. show that the increase in rigid-body rotational entropy on desorption is sufficient to explain the increase of prefactor with increasing chain length [**9**].

Internal vibrations in the alkane molecule such as bond vibrations and angle bending vibrations will be approximately the same whether the molecule is in a bound state on the surface or in a free gas state at the transition state. At the surface, it is possible that some of the other degrees of freedom that are lost due to effects of the surface, such as translation perpendicular to the plane of the surface and the cartwheel rotation, can be treated as vibrations. Since the partition function for vibrations is orders of magnitude less than the partition function for either rigid-body translation or rotation, this increases the prefactor from the "typical" value given by Eq. **3.8**.

$$\frac{k_B T}{h} \qquad \textbf{3.8}$$

The partition function for internal rotations also appears to have an effect on the functionality of the prefactor with chain length. As was discussed above, in a rigid-rod approximation for the alkane molecule [**9**], the increase in rotational entropy with increasing chain length is sufficient to explain the increase in prefactor with increasing chain length. However, alkane molecules have many internal degrees of freedom and can not necessarily be treated as rigid rods. Figure **3-10** shows the fraction of time that a

molecule spends in the all-trans configuration, where none of the carbon backbone torsion angles are in the gauche conformation.

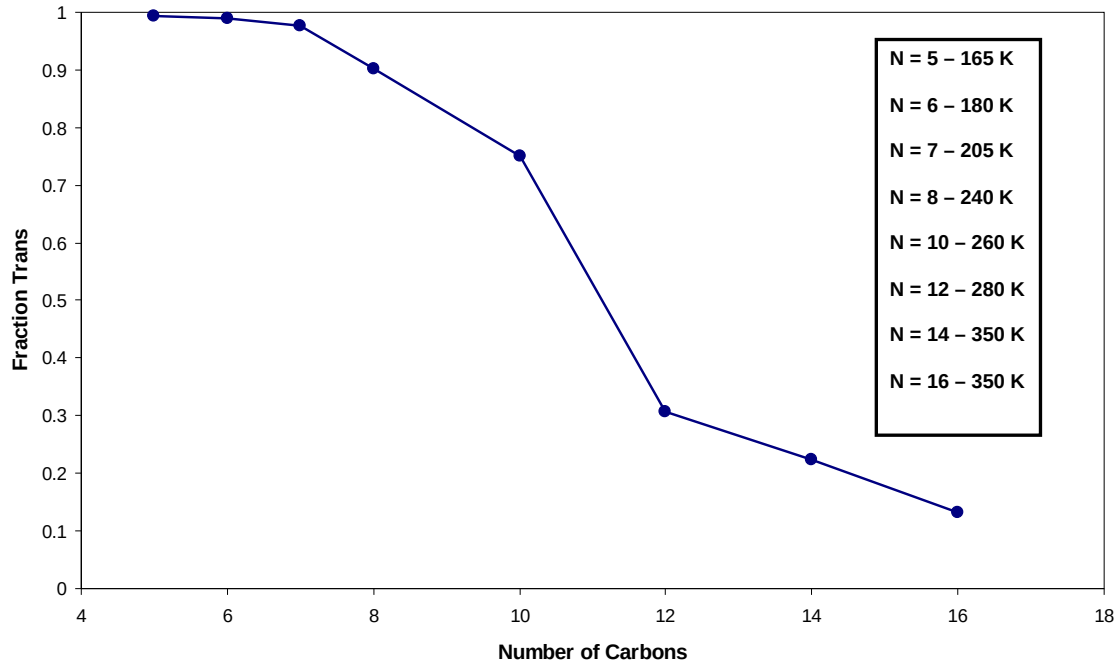

Figure **3-10**: Fraction Trans as a Function of Chain Length

These data points are taken at temperatures near the TPD peak temperature, a temperature where the rate of desorption is very high. For the short alkane molecules (pentane, hexane, and heptane), the desorption temperatures are fairly low. Almost all of the molecules are in the all-trans configuration. These molecules can essentially be treated as rigid rods, and the analysis in [**9**] applies. As the molecule gets longer and subsequently the desorption temperature gets higher, more molecules are found with at least one gauche defect. For molecules longer than decane, the majority of the molecules have at least one gauche defect. As shown in Figure **3-11**, these gauche defects are distributed along the carbon backbone.

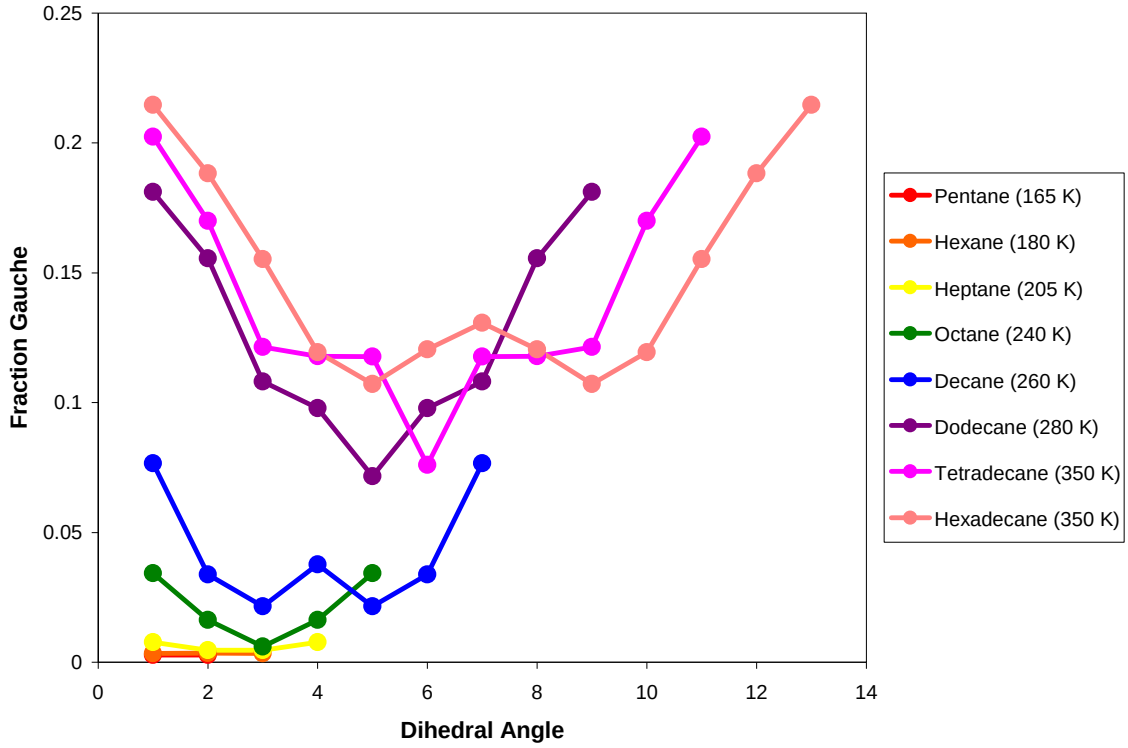

Figure **3-11**: Distribution of Gauche Defects – Variable Chain Length

As would be expected, the carbon backbone angle that is most probable to be found in the gauche conformation is the one that involves the ends of the alkane molecule. However, we note that in the case of hexadecane, even the central backbone angle has a higher probability of being found in the gauche conformation than the end backbone angle of decane. These molecules exhibit rapid trans-gauche conformational changes on the surface, and the effect of q_i can not be ignored. Returning to the entropy formulation of the prefactor as given by Eq. **3.5**, the longer chain molecules with their conformational changes on the surface will have a higher entropy on the surface than would be expected if the molecule was a rigid rod. This decreases the entropy difference from the rigid-rod

value and thus decreases the prefactor from the rigid-rod value. This is shown qualitatively in Figure **3-12**.

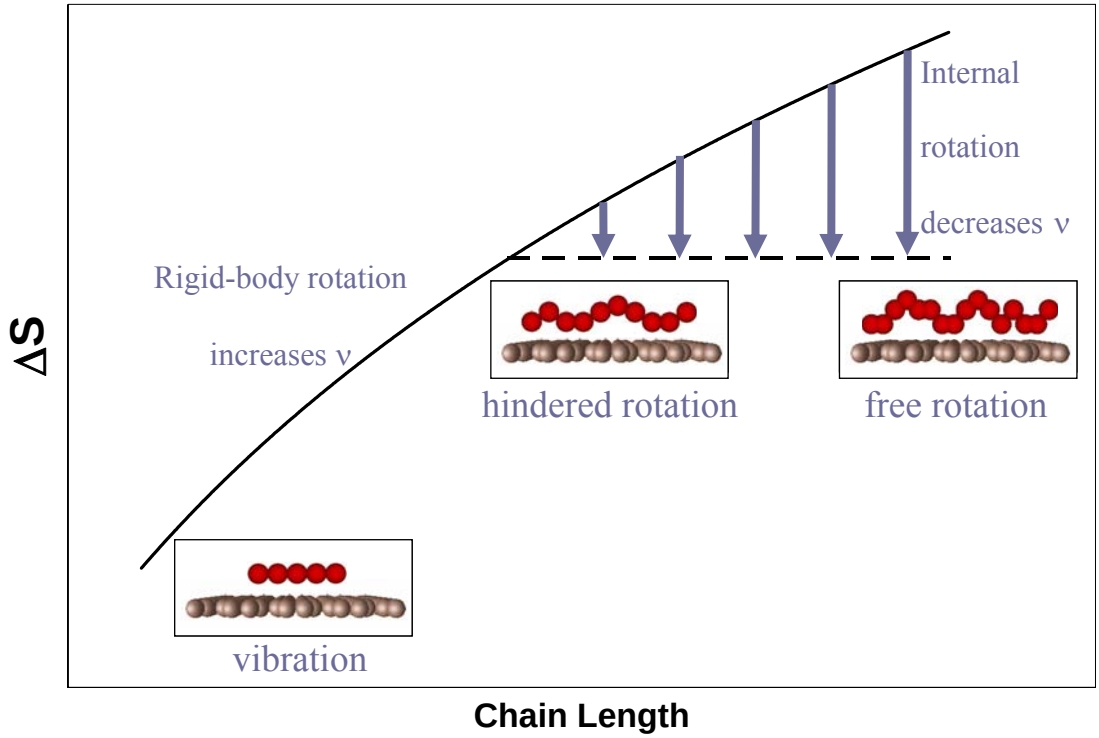

Figure **3-12**: Schematic of the Effect of Chain Length on Entropy and Prefactor

Analysis of the partition function components and entropy definition of the prefactor lead to the conclusion that there are two competing effects causing the functionality of the prefactor with chain length: a chain length effect and a temperature effect (higher temperatures cause more trans-gauche conformational changes). It is beneficial in completing the analysis of the prefactor to separate these two effects. Pentane, at temperatures near the peak desorption temperature of 164 K, is almost always in the trans configuration. However, as is shown in Figure **3-13**, as the temperature of the

simulation is increased past the experimental temperature window, the fraction of pentane molecules that are found in the trans conformation decreases.

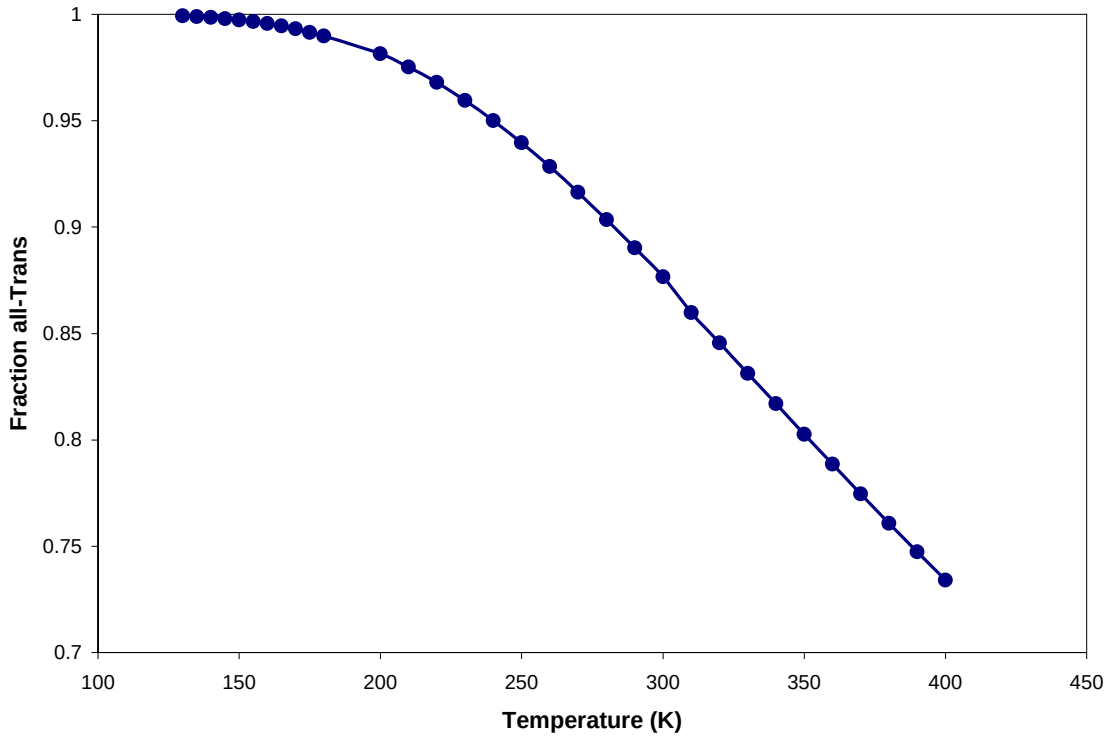

Figure **3-13**: Fraction Trans for Pentane – Variable Temperature

At the highest temperatures, the fraction of pentane molecules in the trans conformation is comparable to the fraction of decane molecules in the trans conformation at experimentally relevant temperatures. Pentane molecules at the graphite surface at the higher temperatures undergo trans-gauche conformational changes. As with the longer molecules at the higher desorption temperatures, this causes the entropy at the surface to be higher than the "expected" value for a rigid-rod. Again, the prefactor takes a lower value than would be expected for a rigid rod. This can also be seen through analysis of the TST rate constants of pentane in two different temperature ranges. The first

temperature range, the experimentally relevant temperature range, is from 130 K to 180 K. Over this temperature range, the pentane molecule spends the majority of the time in the all-trans configuration. The second temperature range is from 300 K to 400 K, which is higher than the experimentally relevant range. In this temperature range, a significant fraction of the pentane molecules have at least one carbon backbone angle in the gauche conformation. The Arrhenius plots for these two temperatures ranges are shown in Figure **3-14**.

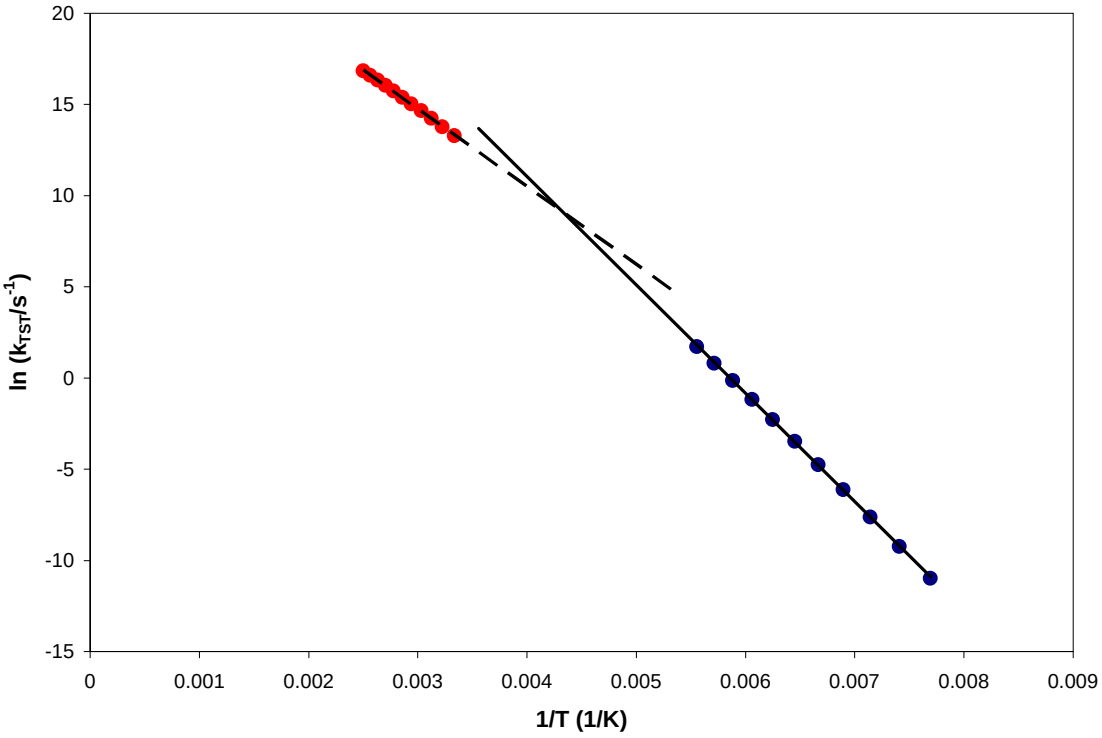

Figure **3-14**: Arrhenius Plot for Pentane – Variable Temperature Range

Extracting the prefactors at these two sets of conditions using Eq. **1.1**, we find that the prefactor changes by three orders of magnitude. The prefactor in the experimentally relevant temperature range is $10^{15.1}$ s^{-1}, while the prefactor in the higher temperature

range is $10^{12.0}$ s^{-1}. This difference in prefactors can be attributed to the different conformations that the pentane molecule can access in the two different temperature ranges.

3.4 Conclusions

The results presented in this chapter represent a comprehensive study on the effect of chain length on desorption at the single molecule (zero coverage) limit. Two different acceleration methods (temperature acceleration and compensating potential) were used and shown to be equivalent for the single molecule case. Due to increased efficiency, the temperature acceleration method was used to study the desorption from the basal plane of graphite of eight different molecules ranging from pentane to hexadecane. Through the acceleration process, we were able to reach physical times of seconds and minutes. These times are inaccessible to conventional MD simulations. Quantifiable measures including desorption energy and prefactor compare favorably to experimental values. The probative power of MD was exploited to examine the molecular state of the desorbing molecules. Conformational changes within the carbon backbones of the molecules were correlated to the functionality of the prefactor with chain length. It was found that short alkane chains which desorb at low temperatures are found mostly in the all-trans configuration. These molecules can be treated as rigid rods, and the prefactor increases with increasing chain length. For longer molecules that desorb at higher temperatures, trans-gauche conformational changes are activated on the surface. The

molecule can no longer be treated as a rigid rod. The entropy of the molecule on the surface is increased from the rigid-rod value, thus decreasing the prefactor from the rigid-rod value. This causes a prefactor that levels off to a constant value at longer chain lengths.

Chapter 4

Pentane Layer Characterization

In order to address some of the issues that were raised in Chapter 3, it is necessary to extend simulations past the single molecule limit to a finite coverage. The work presented in this chapter verifies that the simulated pentane layer exhibits characteristics of an experimental pentane layer and that the results of the accelerated simulations will be physically relevant. Conventional MD simulations were run on a pentane monolayer at various temperatures below experimentally relevant desorption temperatures. The simulations were initialized based on the low-temperature structure as described in [**15**]. The structure of the monolayer was monitored to observe the onset of melting in the pentane layer. These measures were then compared to the experimental melting temperature range of 99 to 105 K [**34**].

4.1 Order Parameter

There are four different kinds of order inherent in a solid pentane monolayer adsorbed on graphite: both translational and rotation order of a pentane molecule with respect to other pentane molecules and both translational and rotational order of a pentane molecule relative to the graphite substrate. When the monolayer melts completely, all of this order will disappear. However, one hallmark of the onset of

melting is the loss of rotational order with respect to the graphite surface. This can be quantified through a set of order parameters defined as

$$OP_n = \frac{1}{N}\left\langle \sum_{i=1}^{N} \cos(n\varphi_i) \right\rangle \qquad \textbf{4.1}$$

where N is the number of molecules in the system, n is related to the symmetry of the solid phase, and φ_i is the angle that the long axis of the molecule makes with the y-axis of the graphite cell [**19**]. As the system loses rotational order with respect to the graphite surface, the full range of angle values will be sampled and the order parameter (regardless of the value of n) will go to zero. The order parameter is calculated for n-values of two, four, six, and eight. At large values of n, the order parameter is sensitive and exhibits larger fluctuations than at small values of n [**19**]. A graph of the order parameter at twelve different temperatures is shown in Figure **4-1**.

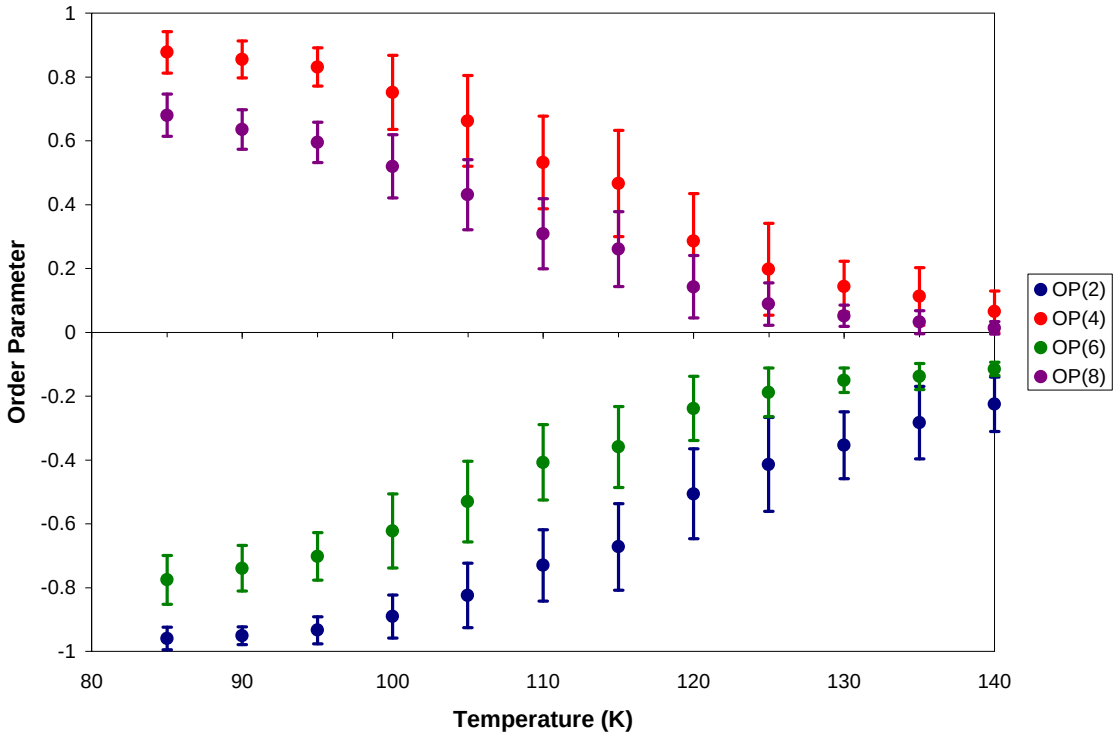

Figure **4-1**: Order Parameter for Pentane Monolayer

As the pentane monolayer begins to melt, values of the order parameters will fluctuate depending on the instantaneous configuration of the system. For configurations that are more liquid-like, the order parameters will be close to zero. If the configuration is more solid-like, the order parameters will have an absolute value close to one. At the melting temperature, both liquid-like and solid-like configurations will exist, increasing the error bars on the order parameters.

As can be seen in Figure **4-1**, the error bars increase in magnitude around 100 or 105 K, and the values for the order parameters start to trend toward a value of zero as temperature increases. This corresponds to the melting temperature of a pentane monolayer of 99 to 105 K [**34**]. When a temperature of 140 K is reached, all of the order

parameters have leveled off near zero, corresponding to a fully melted monolayer. Since the lowest desorption temperatures are above this temperature range, we can deduce that desorption occurs from a liquid state.

4.2 Neutron Scattering

Another measure of the structure of the pentane layer is a neutron scattering profile as a function of wavevector. Experimental data from Kruchten et al. [**15**] show prominent peaks at q-values of approximately 0.7 and 1.4. These q-values correspond to the rectangular unit cell postulated for low temperature pentane configurations.

Neutron scattering intensities can be simulated using a Debye scattering formula [**18**]

$$I(q) = \sum_i \sum_j b_i b_j \frac{\sin(qr_{ij})}{qr_{ij}} \qquad \textbf{4.2}$$

where I(q) is the neutron scattering intensity, b_i and b_j are the neutron scattering lengths for atoms i and j (taken from [**35**]), q is the wavevector, and r_{ij} is the distance between two atoms. The sums are evaluated over all interatomic distances, whether intramolecular or intermolecular. The neutron scattering intensity plots shown in Figure **4-2** were obtained by calculations made at the twelve temperatures from the order parameter simulations.

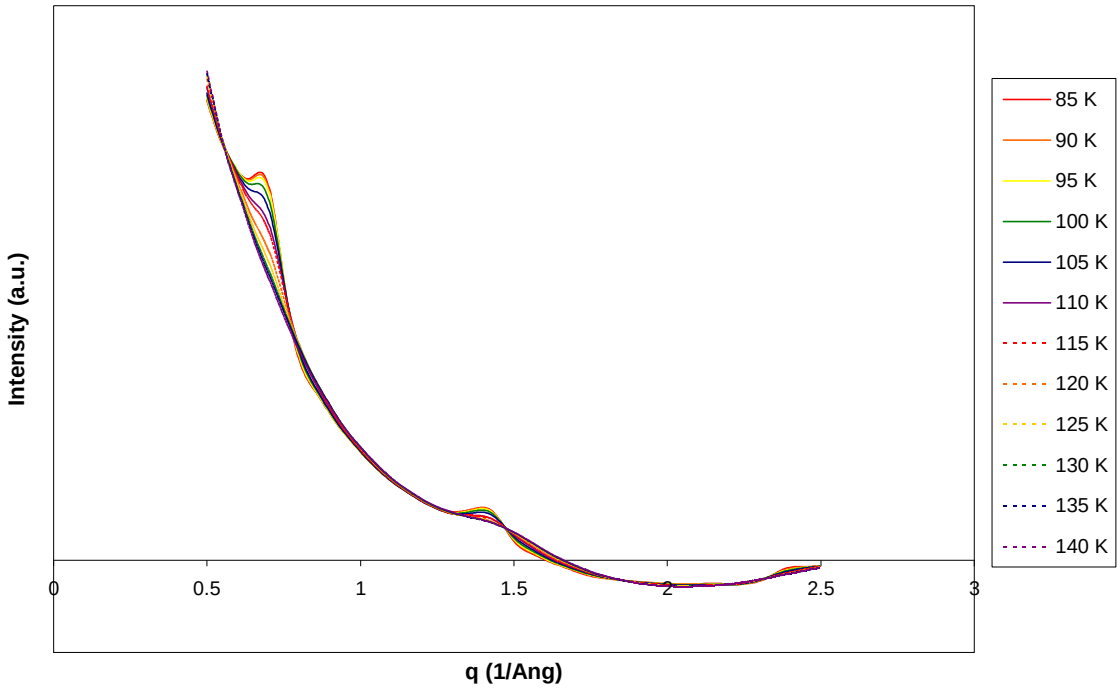

Figure **4-2**: Neutron Scattering Intensity of Pentane on Graphite

At the low temperatures, a prominent peak is evident at q-values of approximately 0.7 and 1.4. These correspond to the molecular configuration proposed in [**15**]. As is discussed in [**18**], the large values corresponding to small q-values are finite size effects. However, their presence does not influence the position of other peaks.

Examining the neutron scattering intensity graphs more closely (Figure **4-3**), it is evident that the peak at a q-value of approximately 0.7 disappears as the temperature increases.

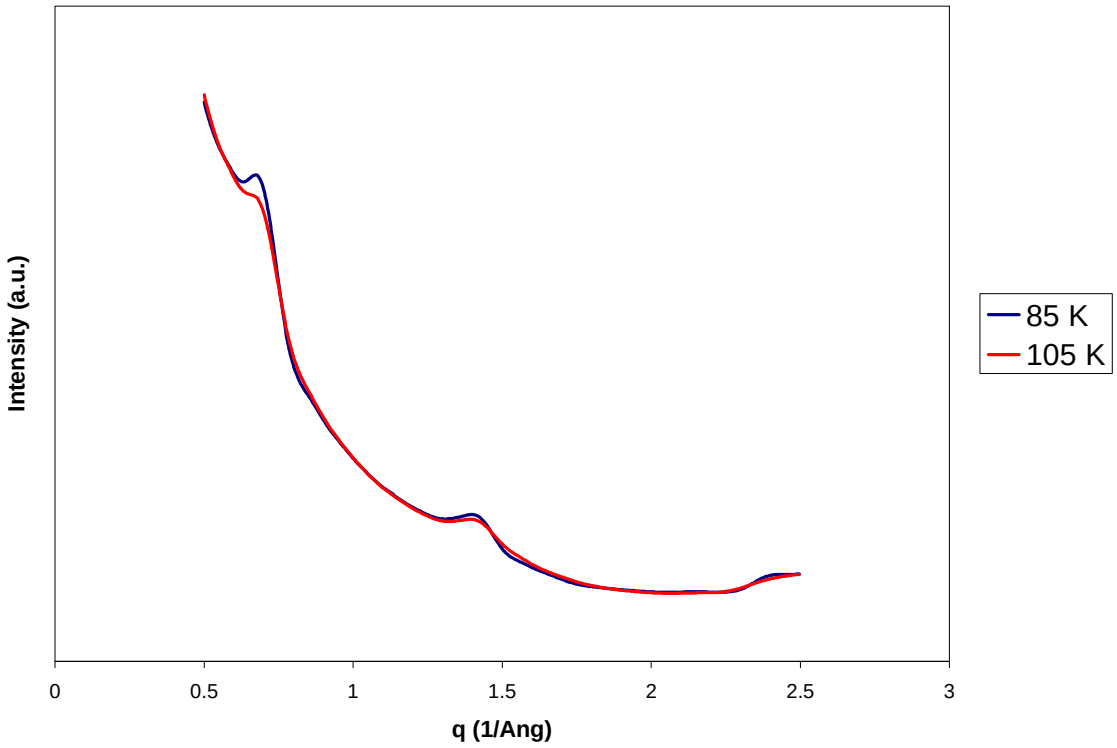

Figure **4-3**: Neutron Scattering Intensity of Pentane on Graphite – Select Temperatures

This is another indication that some of the order in the system has disappeared at a temperature of 105 K. Again, this corresponds to the onset of melting and is in line with the experimental melting temperature [**34**].

4.3 Radial Distribution Function

The radial distribution function is a measure of the order of pentane molecules relative to other pentane molecules. In this case, the radial distribution function is calculated for the center-of-mass distance in the plane of the surface as described in

Section **2.8.2**. The radial distribution functions for the twelve selected temperatures are shown in Figure **4-4**.

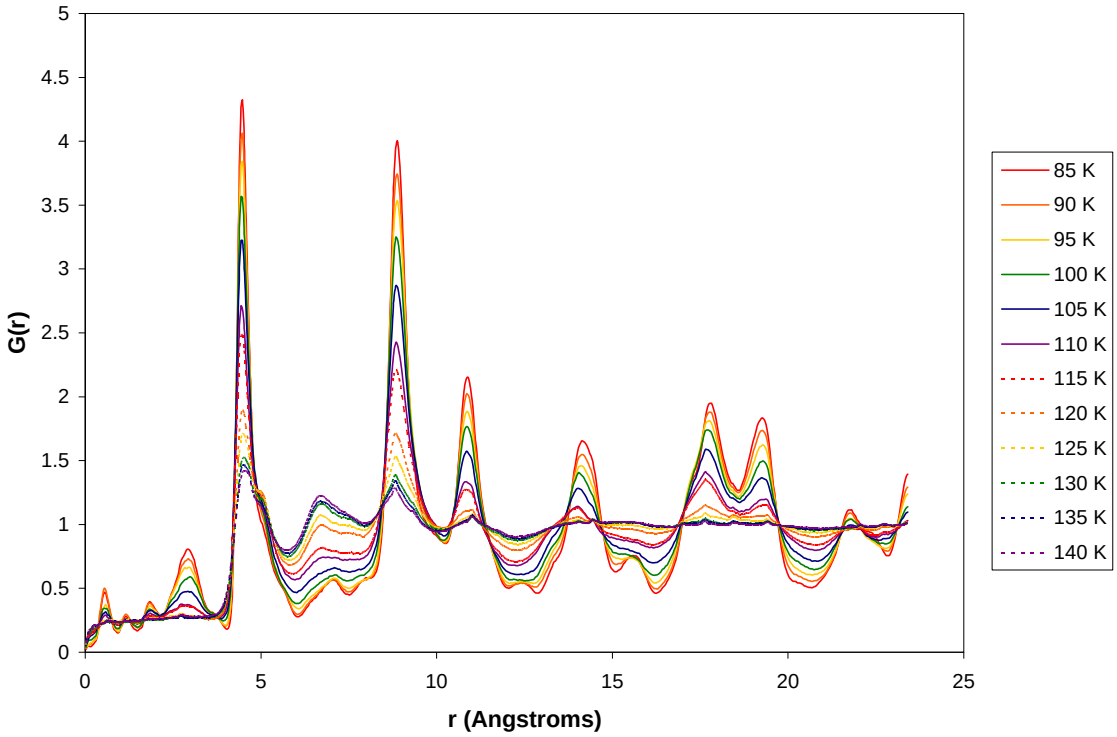

Figure **4-4**: Radial Distribution Function of Pentane on Graphite

Examining the radial distribution function more closely (Figure **4-5**), we see that the order of pentane molecules relative to each other is retained at higher temperatures than the order relative to the graphite surface.

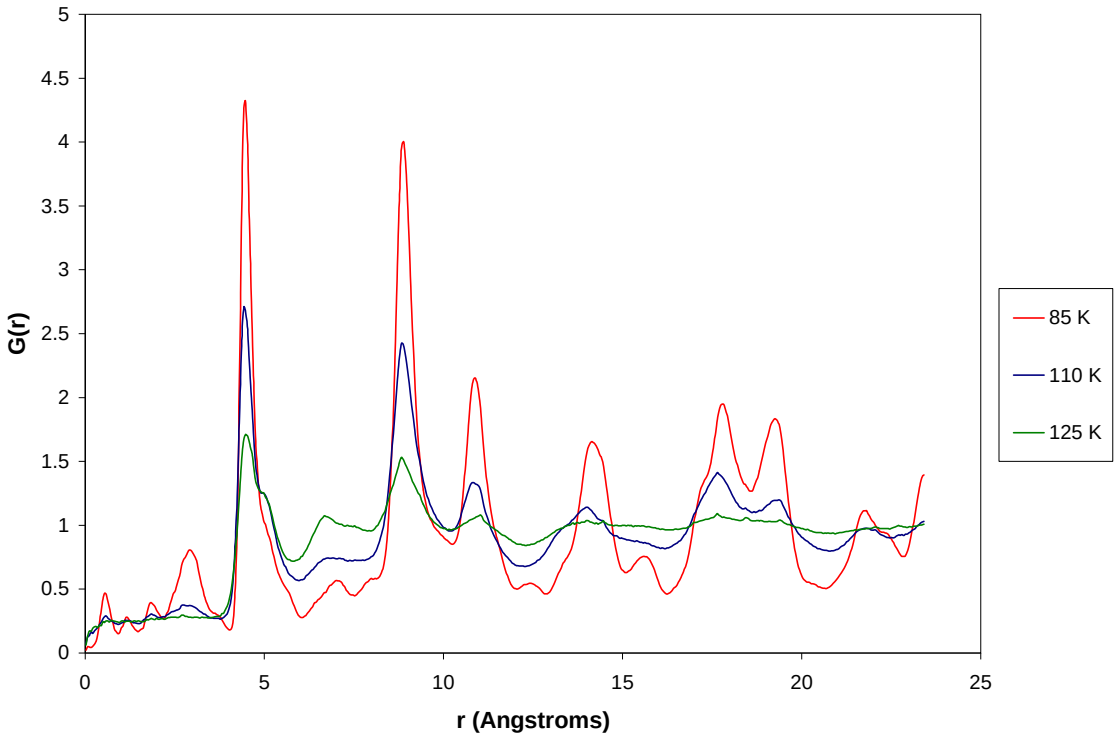

Figure **4-5**: Radial Distribution Function of Pentane on Graphite – Select Temperatures

At 110 K, peaks corresponding to close-range order have almost completely disappeared while those at long-range are still present. When the temperature is increased to 125 K, most of the long-range order peaks have also disappeared, indicating a loss of order of pentane molecules relative to each other.

4.4 Conclusions

Simulations to characterize the pentane layer have been run using conventional MD. Various quantities such as order parameters, neutron scattering intensities, and radial distribution functions are used to probe the onset of loss of order in the pentane

monolayer. Order parameter simulations show the onset of loss of rotational order of the pentane molecules relative to the graphite surface at a temperature around 100 to 105 K. Neutron scattering intensity simulations show a loss of the peak at a q-value of approximately 0.7 at a temperature of 105 K. Radial distribution function simulations characterize the loss of translational order of pentane molecules relative to each other. Short-range order is lost around the experimental melting temperature of 105 K. However, long-range order persists to higher temperatures. In all cases, order was lost at temperatures well below the peak desorption temperature of 164 K, showing that the desorption of pentane from the basal plane of graphite occurs from a liquid state.

Chapter 5

Variable Coverage Simulations

Although single molecule simulations can provide insight to the desorption process, experiments involve finite coverages of molecules. Experimental analyses often assume that the results obtained are coverage independent. However, if intermolecular interactions are significant, this will not be the case. Thus, it is necessary to examine the effect of intermolecular interactions on desorption energy and prefactor to validate this assumption. In this chapter, we present accelerated MD simulations that examine the role of coverage and desorption environment on desorption rate.

5.1 Acceleration Method

The acceleration of the desorption process is based on the bond-boost method of Miron and Fichthorn [**4**]. The bond-boost creates a modified potential energy surface based on an empirical form for ΔV and a physical description of the transition state. The generic form of ΔV is

$$\Delta V = \frac{A(\varepsilon_{\max})}{N} \sum_{i=1}^{N} \delta V_i \qquad \textbf{5.1}$$

where $A(\varepsilon_{max})$ is an empirical envelope function that forces the boost potential to zero at the transition state, N is the number of alkane molecules in the simulation, and δV_i is a

boost potential added to each individual alkane molecule. The simple picture of the desorption process leads to a very intuitive description of the transition state. As in the single molecule simulations, the transition state is defined when one molecule has reached a height above the graphite surface where the interaction between the molecule and the surface is negligible.

The boost potential applied to each molecule δV_i is chosen to facilitate the desorption process. One can imagine increasing the rate of desorption in a simple manner by decreasing the molecule-surface interaction by filling in that potential with a compensating potential. This leads to δV_i of the form

$$\delta V_i = \alpha V_{s,i} \qquad \textbf{5.2}$$

where $V_{s,i}$ is the molecule-surface interaction for molecule i and α is an empirical parameter between 0 and 1 that controls the extent of acceleration. However, as with the single molecule compensating potential acceleration scheme, the modified molecule-surface potential energy becomes comparable in magnitude to other interactions in the system. In this case, the modified molecule-surface interaction became the same order of magnitude as the intermolecular interactions. This caused non-physical effects in the simulation, such as the formation of three-dimensional islands. To solve the problem, a second term was added to δV_i to decrease the intermolecular interactions. Therefore, the new δV_i took the form

$$\delta V_i = \alpha_1 V_{s,i} + \alpha_2 V_{\text{int},i} \qquad \textbf{5.3}$$

where α_1 and α_2 are separate parameters to control the extent of boost in the molecule-surface interactions and intermolecular interactions respectively and $V_{int,i}$ is the intermolecular interaction for molecule i.

The envelope function, $A(\varepsilon_{max})$, serves two distinct functions that help improve the efficiency of the bond-boost method. It is defined as

$$A(\varepsilon_{\max}) = 1 - \left(\frac{\varepsilon_{\max}}{q}\right)^2; \quad \varepsilon_{\max} < q \qquad \textbf{5.4}$$

where q is an empirical threshold that determines when in the simulation the boost is applied and ε_{max} is a measure of how far the system is from an equilibrium configuration. Mathematically, ε is defined as

$$\varepsilon = \frac{z_{com,i} - z_{eq}}{z_{eq}} \qquad \textbf{5.5}$$

where $z_{com,i}$ is the distance of the center-of-mass from the surface, perpendicular to the surface, of molecule i, and z_{eq} is the preferred binding distance of the alkane molecule from the surface. Physically, this means that ε is a measure of how far a molecule is from desorbing. ε_{max} is the value of ε that is a maximum, corresponding to the molecule that is closest to desorbing. The threshold, q, is normalized by the preferred binding distance and chosen below the transition state height. Since the value of A is zero if q is greater than ε_{max}, the form of A ensures that the boost potential ΔV will be zero at the desorption transition state.

The second function of A is to funnel the boost into the molecule that is closest to desorbing. This can be seen by examining the forces that are exerted on each of the

molecules on the modified potential energy surface. The force on each atom is determined by the derivative of the potential energy, taken on the modified potential energy surface. This can be written mathematically as

$$F_i = -\frac{\partial V^*}{\partial r_i} = -\frac{\partial V}{\partial r_i} - \frac{\partial \Delta V}{\partial r_i} \qquad \textbf{5.6}$$

The force can be broken down as a force derived from the actual potential energy surface and an additional term derived from the boost potential. With a boost potential of the form in Eq. **5.1**, this second force term can be written as

$$-\frac{\partial \Delta V}{\partial r_i} = -\frac{A}{N}\frac{\partial}{\partial r_i}\left(\sum_{i=1}^{N} \delta V_i\right) - \frac{\partial A}{\partial r_i}\left(\frac{1}{N}\right)\sum_{i=1}^{N} \delta V_i \qquad \textbf{5.7}$$

All of the molecules will experience the extra force provided by the first term in Eq. **5.7**. However, A depends only on the position of the molecule that is closest to desorbing. So, its derivative with respect to atoms will be non-zero if and only if the atoms are in the molecule that is closest to desorbing. This second term provides an extra force acting only on the molecule that is closest to desorbing, thus funneling extra boost into that molecule. Values for z_{eq}, q, α_1 and α_2 can be found in Table **5-1**.

Table **5-1**: Parameter Values for Layer Acceleration

Parameter	Value
z_{eq}	3.444 Å
Q	2.57
α_1	0.1
α_2	0.35

5.2 Method Validation

As with the single molecule simulations, it is vital to preserve the relevant physics of the system on the modified potential energy surface. The same range of energies must be sampled in both a conventional MD simulation and an accelerated simulation of the same conditions. However, in the case of layer simulations, simply sampling the same range of total energy is insufficient to ensure that the configuration of the system is preserved by the acceleration. The energy must be correctly partitioned between the three major types of energy: intramolecular, intermolecular, and molecule-surface. The histograms for each type of energy are collected as described in Section **2.8.1**. Figure **5-1** shows a sample set of energy histograms. These histograms overlap almost exactly, showing that the modified potential energy surface preserves the equilibrium energy distributions that occur on the actual potential energy surface.

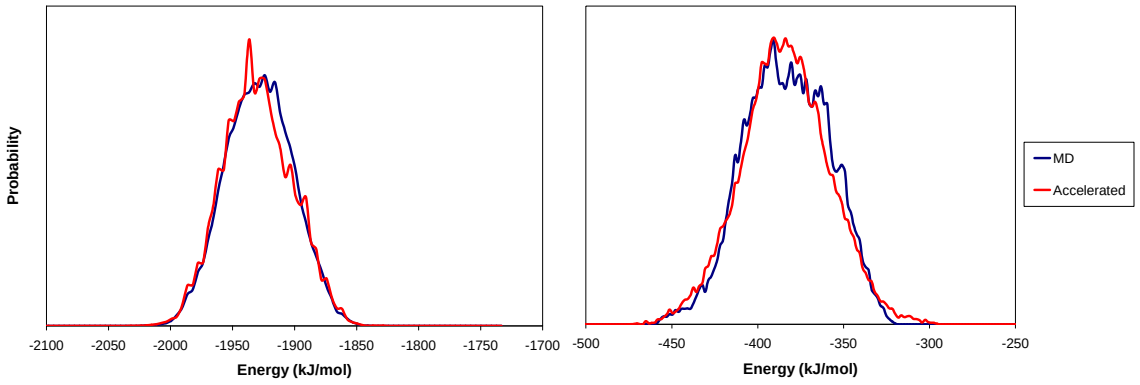

Figure **5-1**: Energy Histograms for Pentane Desorbing from the Basal Plane of Graphite: From Left to Right: Molecule-Surface Energy for Monolayer Coverage at 160 K, Intermolecular Energy for 0.5 Monolayer Coverage at 160 K

One reason for using the bond-boost method instead of the highly efficient temperature acceleration method is to preserve the structure inherent in the layer on the modified potential energy surface. The layer structure is characterized by the radial distribution function of the center-of-mass of the alkane molecules as described in Section **2.8.2**. A characteristic radial distribution function is shown in Figure **5-2**. It is evident that the structure of the layer in the conventional MD simulation is the same as the structure of the layer in the accelerated simulation. The peaks are at the same distance values, indicating that the structure has the same length scale in both the conventional MD and the accelerated system. Furthermore, the peaks have the same relative magnitude between the conventional MD and the accelerated system.

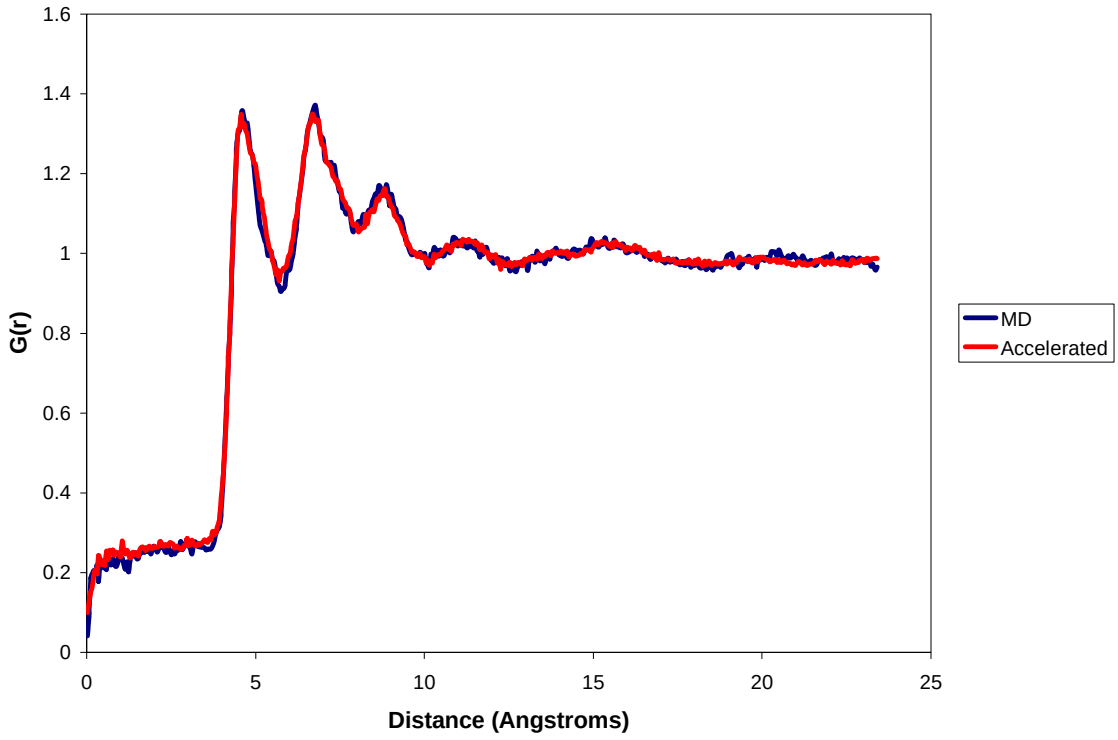

Figure **5-2**: Radial Distribution Function of Pentane on Graphite – 0.75 Monolayer, 170 K

Another measure for comparing the accelerated system to the conventional MD system is the roll angle. As discussed in Section **2.8.3**, this is the angle between the plane of the alkane molecule and the plane of the graphite surface. An angle of 0 or 180 degrees corresponds to a molecule lying flat with the backbone parallel to the surface. An angle of 90 degrees corresponds to a molecule tipped up with the backbone perpendicular to the surface. As the molecule tips up in the layer simulation, the molecule-surface interaction decreases while the intermolecular interaction increases. So, the roll angle reflects the balance between these two interactions. If the acceleration scheme does not preserve this balance, it would be reflected in differences in the roll angle between the conventional MD simulation and the accelerated simulation. A characteristic roll angle distribution is shown in Figure **5-3**. The most probable configuration for the molecule is lying flat with the backbone parallel to the surface. A small bump in the probability occurs when the molecule is tipped perpendicular to the surface, although this probability is over an order of magnitude less than the probability for a flat molecule. This bump in probability is also seen in simulations of hexane on graphite [**18**].

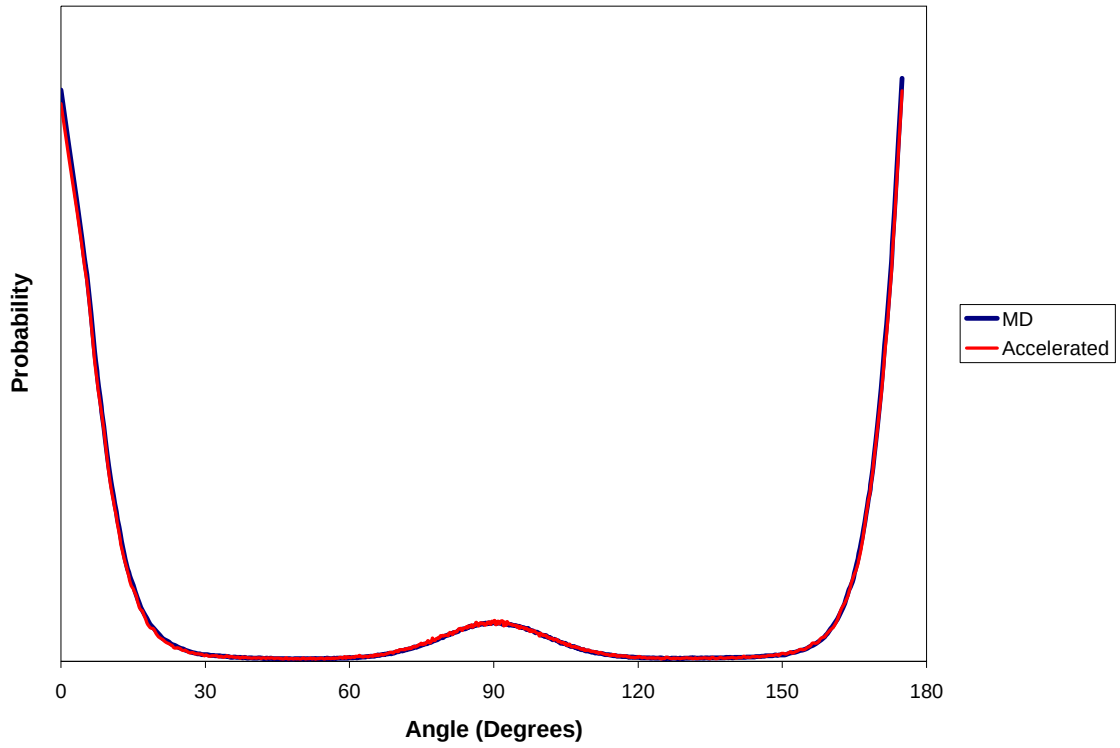

Figure **5-3**: Roll Angle Distribution for Pentane on the Basal Plane of Graphite – Monolayer Coverage at 170 K

5.3 Arrhenius Plots

The desorption of pentane molecules from layers of fixed coverage is assumed to follow the form of Eq. **1.1**. The layer is initialized based on the unit cell for pentane on graphite as described by Kruchten et al. [**15**]. It is equilibrated for 200 picoseconds at the temperature of interest on the actual potential energy surface. The desorption simulation is run on the modified potential energy surface, and averages are accumulated according to Eq. **2.29**. Once the molecule has passed through the desorption transition state, the

simulation ends. Rates are collected for five different temperatures ranging from 160 K to 180 K with an interval of 5 K. Coverages include a full monolayer (ML), as defined by the number of pentane molecules for the number of graphite unit cells as described in [**15**], along with 0.25, 0.5, and 0.75 ML. Arrhenius plots are shown in Figure **5-4** for all coverages and temperatures. Analyses of the Arrhenius plots are based on Eq. **1.1**. A summary of the desorption energy and prefactor for each coverage is shown in Table **5-2**.

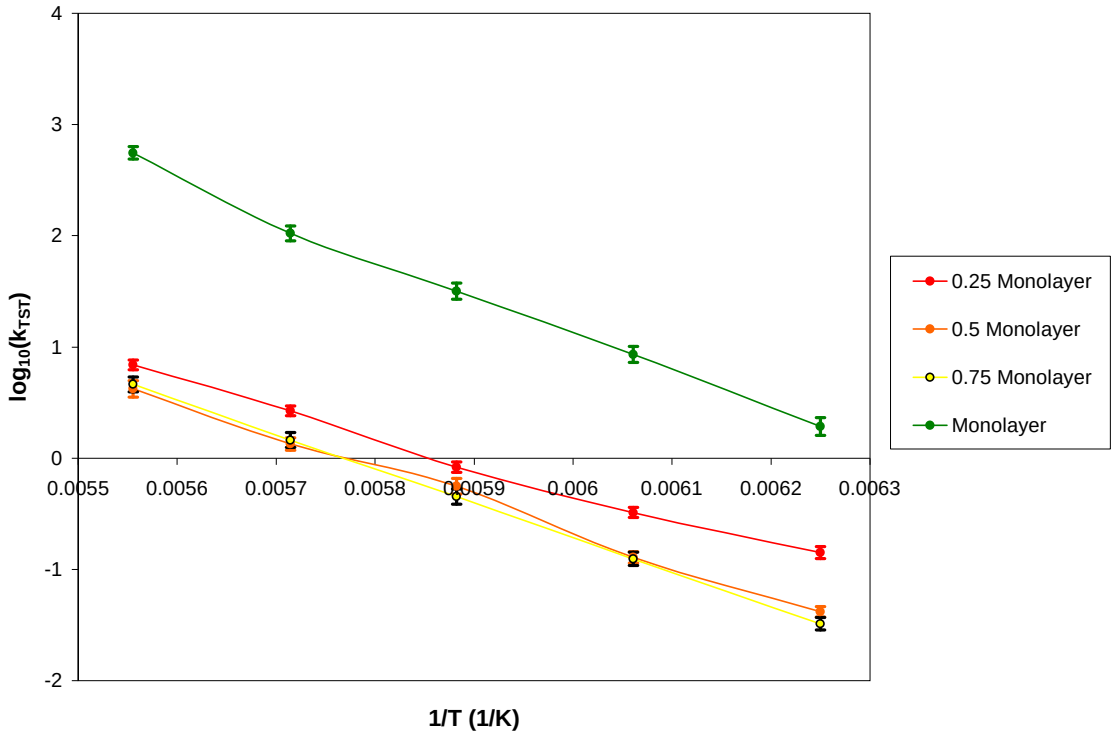

Figure **5-4**: Arrhenius Plots of the Desorption of Pentane from the Basal Plane of Graphite – Variable Coverage

Table **5-2**: Desorption Parameters – Variable Coverage Simulations

Coverage	Desorption Energy (kJ/mol)	$Log_{10}(\nu)$ (1/s)
0.25 ML	47 ± 3	15 ± 1
0.50 ML	55 ± 4	17 ± 1
0.75 ML	59 ± 4	18 ± 1
1.0 ML	66 ± 5	22 ± 1

The most surprising result derived from these simulations is the fact that the desorption rate from a monolayer is higher than the desorption rate from the submonolayer coverages. The desorption rate decreases from the monolayer to 0.5 ML coverage. Then, the rate increases again for 0.25 ML coverage. There are two major components that contribute to the magnitude of the rate, as can be seen by examining Eq. **1.1**: the prefactor (ν) and the desorption energy (E_D). A high rate can be the consequence of either a low desorption energy or a high prefactor. As can be seen in Table **5-2**, both the prefactor and the desorption energy increase with increasing coverage. In the case of 0.25 ML, the desorption energy is lower than the other coverages. A snapshot of the molecular configuration at 0.25 ML (Figure **5-5**) shows that the molecules have many fewer neighbors than at higher coverages.

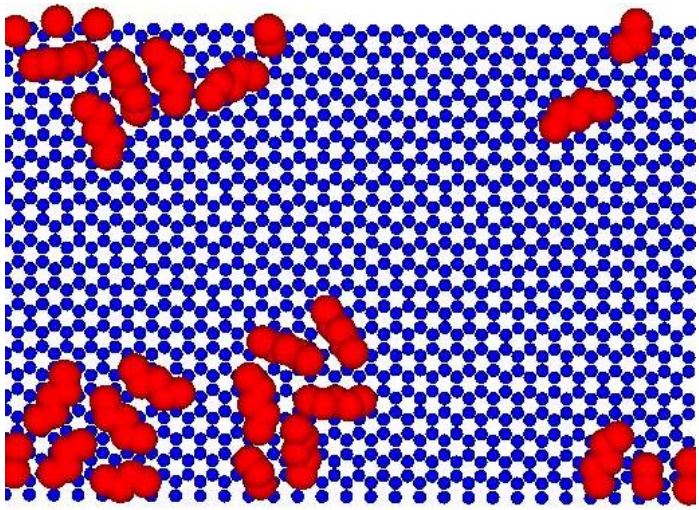

Figure **5-5**: Molecular Configuration of Pentane on the Basal Plane of Graphite at 0.25 ML and 165 K

The attractive intermolecular forces are lessened, and the desorption energy is decreased. At the other extreme, molecules in the monolayer have many neighbors and large attractive intermolecular interactions. This results in greater desorption energies than at the lower coverages. However, since there are fewer ways to place a full monolayer on the graphite surface, the monolayer (shown in Figure **5-6**) is more ordered when compared to the lower coverages.

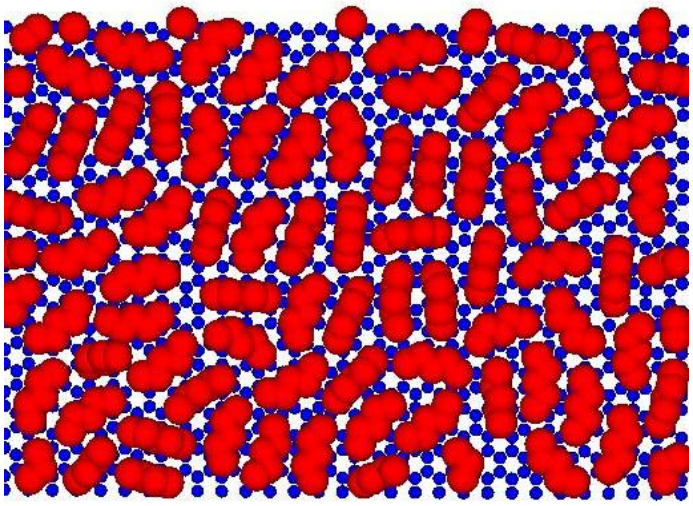

Figure **5-6**: Molecular Configuration of Pentane on the Basal Plane of Graphite at Monolayer and 165 K

From Section **3.3**, the prefactor is related to the change in entropy upon desorption according to Eq. **3.5**. With many neighbors, molecules on the surface are restricted, and the entropy on the surface is higher than the entropy at lower coverages. This increases the entropy difference between the molecule on the surface and the molecule at the transition state compared to the entropy difference for a molecule at a lower coverage. The increased entropy difference is reflected in a larger prefactor, which leads to a high rate. So, the high rate associated with the monolayer coverage is a result of entropic forces. An entropic repulsion forces molecules out of the monolayer at a rate that is higher than would be expected by energetics alone. This balance between energy and entropy causes the rate to go through a minimum at intermediate coverages between a full monolayer and zero coverage. At low coverages, the rate is dominated by low desorption energies. At high coverages, the rate is dominated by the large prefactor that results from large changes in entropy upon desorption.

5.4 Conclusions and Recommendations

We examined the desorption of pentane from the basal plane of graphite at a variety of coverages and temperatures. Accelerated MD is used to extend the timescale of the simulation to experimentally relevant times at experimentally relevant temperatures. The accelerated MD method is based on the bond-boost method of Miron and Fichthorn [**4**] and accelerates the simulation by decreasing the molecule-surface and intermolecular interactions. Physical quantities in the simulation such as various forms of energy, radial distribution functions and pentane roll angle are compared to those obtained from conventional MD to ensure that the physics of the system are preserved. The results show that the desorption rate decreases from a monolayer coverage simulation to intermediate coverage simulations and then increases again at low coverages. This is attributed to a balance between energy and entropy in the system. At low coverages, low desorption energies lead to high rates. As the coverage increases, molecules experience more attractive intermolecular forces and the desorption energy increases, whereby the rate is decreased. At monolayer coverages, entropy differences between a molecule on the surface and a molecule at the transition state as reflected in the prefactor dominate the rate expression and cause it to increase again.

The question of the balance between energy and entropy warrants further study. By simulating more submonolayer coverages, the transition between entropy-dominated and energy-dominated regimes of desorption rate can be determined. If enough

submonolayer coverages were simulated, it would be possible to create an accurate function that relates desorption rate to both coverage and temperature. This function could then be used to simulate TPD based on previously defined analyses.

In addition, it is clear that the desorption environment affects the desorption energetics. More measures of the configurations of individual molecules and the layer as a whole would shed light on the dominant desorption environments and the effect of alternate environments on desorption energy and prefactor.

Chapter 6

Temperature Programmed Desorption Simulations

Temperature programmed desorption (TPD) is an experimental technique commonly used to study the kinetics of surface processes. A solid surface is prepared by heating it to remove any contaminants that may be adsorbed. It is then placed in an ultra-high vacuum chamber. A known amount of vapor is introduced to the chamber and adsorbs to the solid surface. After adsorption is complete, the temperature of the surface is ramped linearly with time according to the equation

$$T = T_o + \beta t \qquad \textbf{6.1}$$

where T_o is the temperature at the beginning of the experiment, β is the heating rate (usually in K/s), and t is the time elapsed during the experiment. The intensity of molecules desorbing from the solid surface is monitored using a mass spectrometer. The plot of this intensity versus the time elapsed (or equivalently the temperature of the surface) is referred to as a TPD profile. A sample TPD profile is shown in Figure **6-1**. The temperature corresponding to a local maximum in the TPD profile is referred to as the peak desorption temperature, T_p.

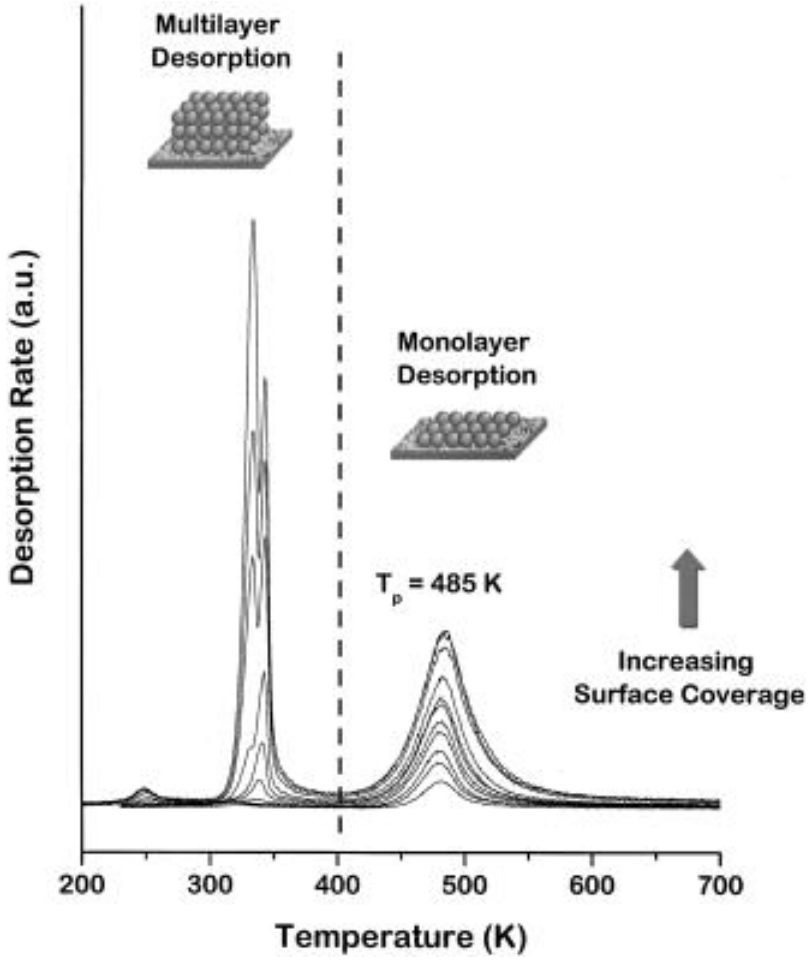

Figure **6-1**: Sample TPD profile from [**5**]

In general, analysis of a TPD profile is based on ideas put forth by Redhead [**20**]. It assumes a simple power law expression for the desorption rate

$$r_d = -\frac{\partial \theta}{\partial t} = \nu \theta^n \exp\left(-E_D / k_B T\right) \qquad \textbf{6.2}$$

where r_d is the rate of desorption, θ is the fractional coverage of the desorbing species, ν is the prefactor, n is the order of the desorption process, and E_D is the desorption energy. Combining this expression for the rate with the temperature-ramping expression from Eq. **6.1** yields an expression for the rate in terms of the temperature

$$\frac{r_d}{\beta} = -\frac{\partial \theta}{\partial T} = \frac{\nu}{\beta}\theta^n \exp\left(-E_D / k_B T\right) \qquad \textbf{6.3}$$

6.1 TPD Simulation Set-Up

Eq. **6.3** is the basis for our accelerated MD simulations of TPD. The graphite surface is filled with pentane molecules and equilibrated with a conventional MD simulation to 140 K, a temperature below the onset of desorption in experiments. At this point in the simulation, the acceleration is activated. Molecules are allowed to move on the modified potential energy surface as defined in Section **5.1**. The physical time is advanced according to Eq. **2.26**, and the temperature is changed continuously based on the input heating rate. As each molecule desorbs, the time to desorption is recorded, and the molecule is removed from the system. An equilibration period of 50 picoseconds using conventional MD is added after each desorption to ensure that the assumptions inherent in TST as discussed in Section **2.6** (specifically that the reactant state is in equilibrium) are fulfilled. Once all of the molecules in the simulation have desorbed, a plot of coverage (or number of molecules) versus time (or temperature) can be created. A sample plot is shown in Figure **6-2**.

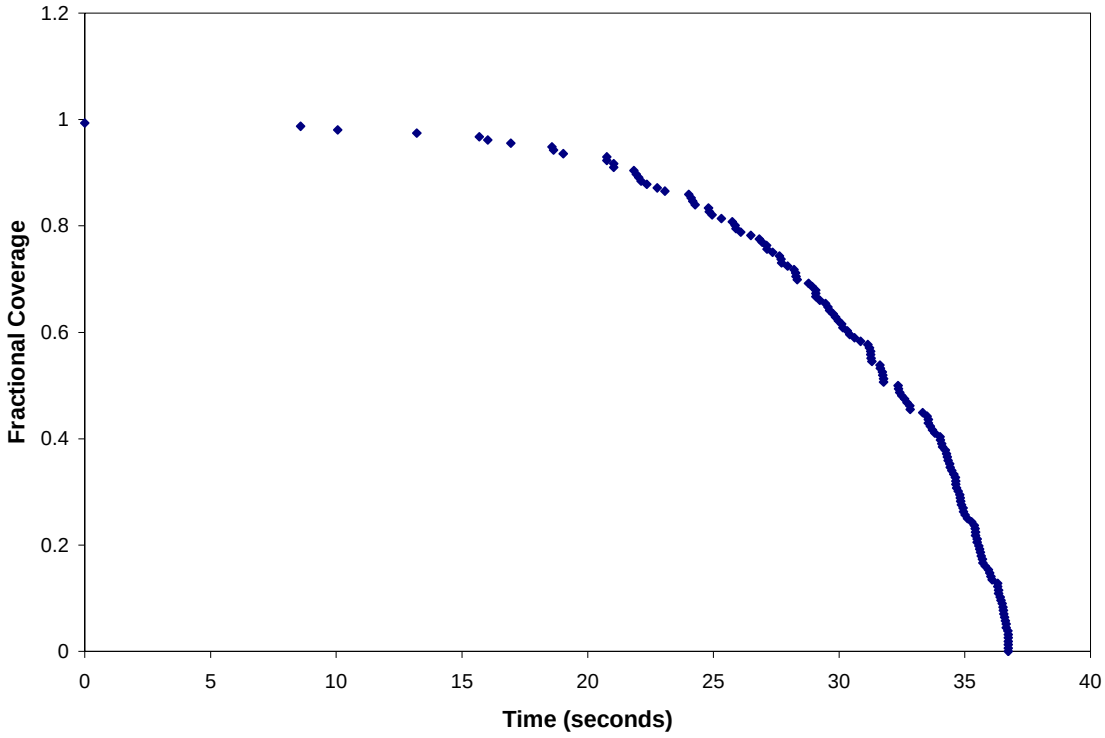

Figure **6-2**: Characteristic Plot of Fractional Coverage versus Time – Monolayer Coverage, $\beta = 0.6$ K/s, Single Simulation

The TPD simulation is run for multiple starting configurations, and the results of desorption time are combined to create a single plot of number of molecules versus time, shown in Figure **6-3**.

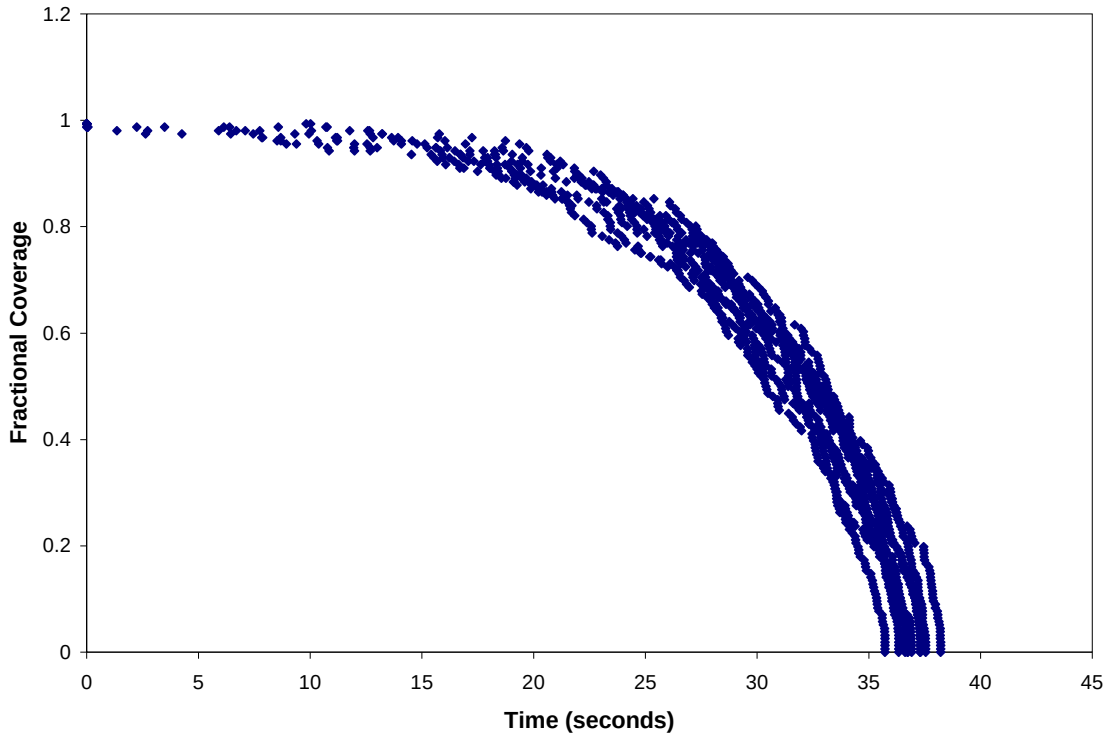

Figure **6-3**: Fractional Coverage versus Time – Monolayer Coverage, β = 0.6 K/s, Multiple Simulations

The time resolution in a TPD experiment is governed by the heating rate. For fast experimental heating rates (2 K/s or 5 K/s), time resolution of the mass spectrometer can be on the order of milliseconds. For slower heating rates (less than 1 K/s), the time resolution of the mass spectrometer is on the order of seconds. Since the simulations can provide time resolution on the order of femtoseconds, it is important to analyze the simulation results with the experimental resolutions in mind. Simulation results are grouped in "blocks" corresponding to the experimental resolution timescales. These blocks are then averaged to produce a plot of average number of molecules versus time

that reflects experimental resolution limitations. A sample average plot is shown in Figure **6-4**, superimposed on the full plot that produced the averages.

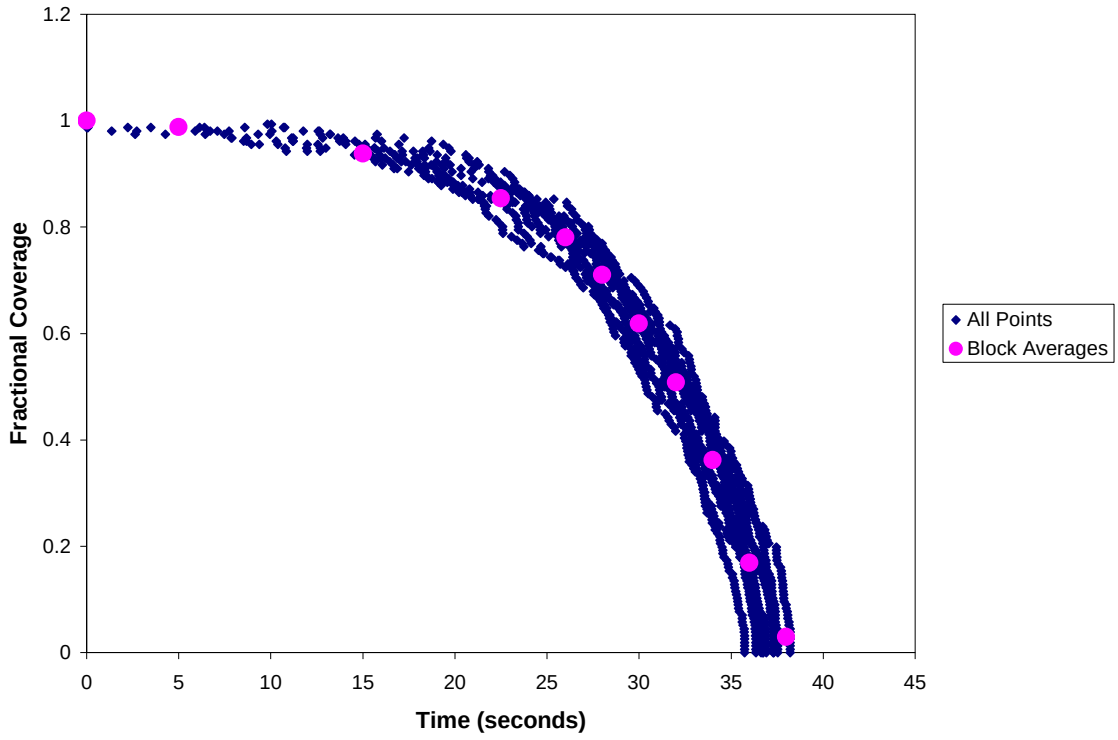

Figure **6-4**: Fractional Coverage versus Time – Monolayer Coverage, β = 0.6 K/s, Multiple Simulations and Block Averages

From these averages, the derivative in Eq. **6.2** can be evaluated. This derivative plotted against the temperature gives a TPD profile. The peak temperature of each profile can be extracted along with the desorption energy and prefactor for the desorption of pentane from graphite. A sample TPD profile is shown in Figure **6-5**.

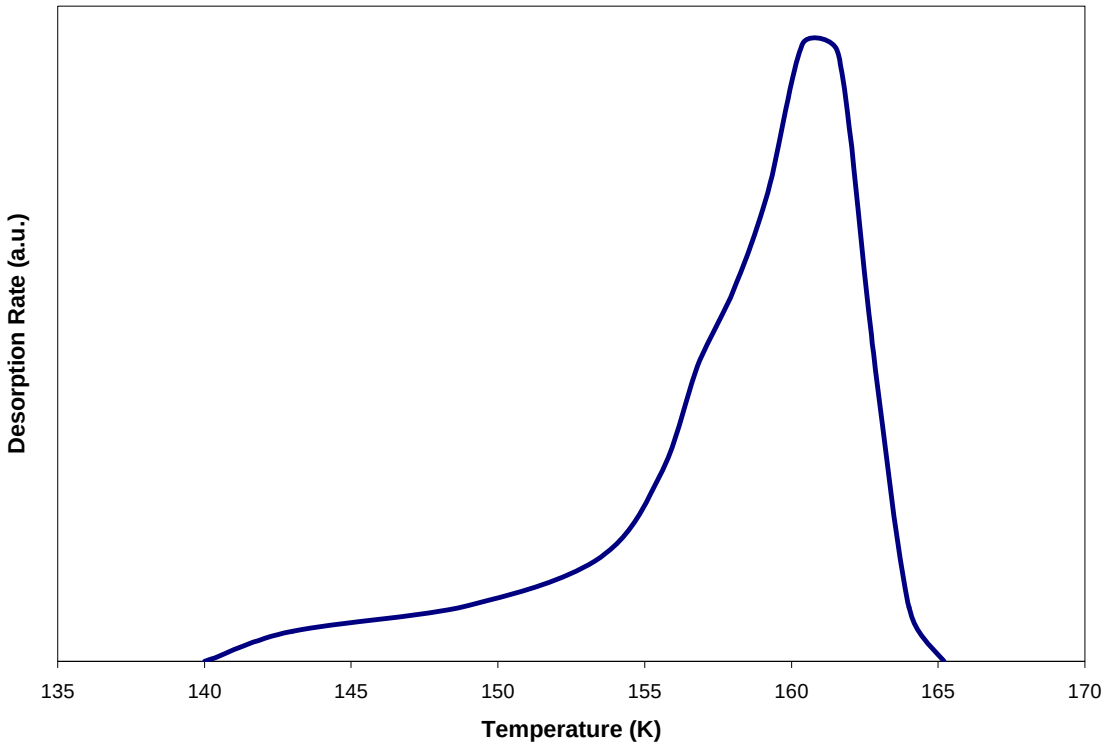

Figure **6-5**: TPD Profile – Monolayer Coverage, β = 0.6 K/s

Extracting the desorption energy and prefactor from a TPD profile is also based on Redhead analysis [**20**]. Many of the experimental results assume that the desorption of alkanes is a first-order process [**5, 8-10**]. We use this same assumption in analyzing the TPD profiles from the accelerated MD simulations. For first order desorption, Eq. **6.3** simplifies to

$$\frac{r_d}{\beta} = -\frac{\partial\theta}{\partial T} = \frac{\nu}{\beta}\theta\exp\left(-E_D / k_B T\right) \qquad \textbf{6.4}$$

At the peak temperature, the desorption rate is at a maximum. Thus, differentiating Eq. **6.4** while assuming that the desorption energy and prefactor are

independent of temperature yields an equation that relates the prefactor, desorption energy, peak temperature, and heating rate

$$\ln\left(\frac{\nu}{E_D}\right) - \frac{E_D}{k_B T_p} = \ln\left(\frac{\beta}{k_B T_p^2}\right) \qquad \textbf{6.5}$$

where T_p is the peak temperature. Simulations are run at various values of β, and the values for T_p for each β are recorded. From Eq. **6.5**, a plot of $1/T_p$ versus $\ln(\beta/T_p^2)$ is a straight line with a slope of $-E_D/k_B$. From the calculated value of E_D, the value of ν can be calculated using an average of values from Eq. **6.5**.

6.2 TPD with Variable Initial Coverage

The first set of TPD results are at a fixed heating rate while varying the initial coverage. Results at a heating rate of 0.6 K/s provides a comparison with experimental TPD results. Tait et al. examined the desorption of butane and hexane on the basal plane of graphite at initial coverages of both a full monolayer and submonolayers [**10**]. The simulation results for pentane, shown in Figure **6-6**, have many of the same features.

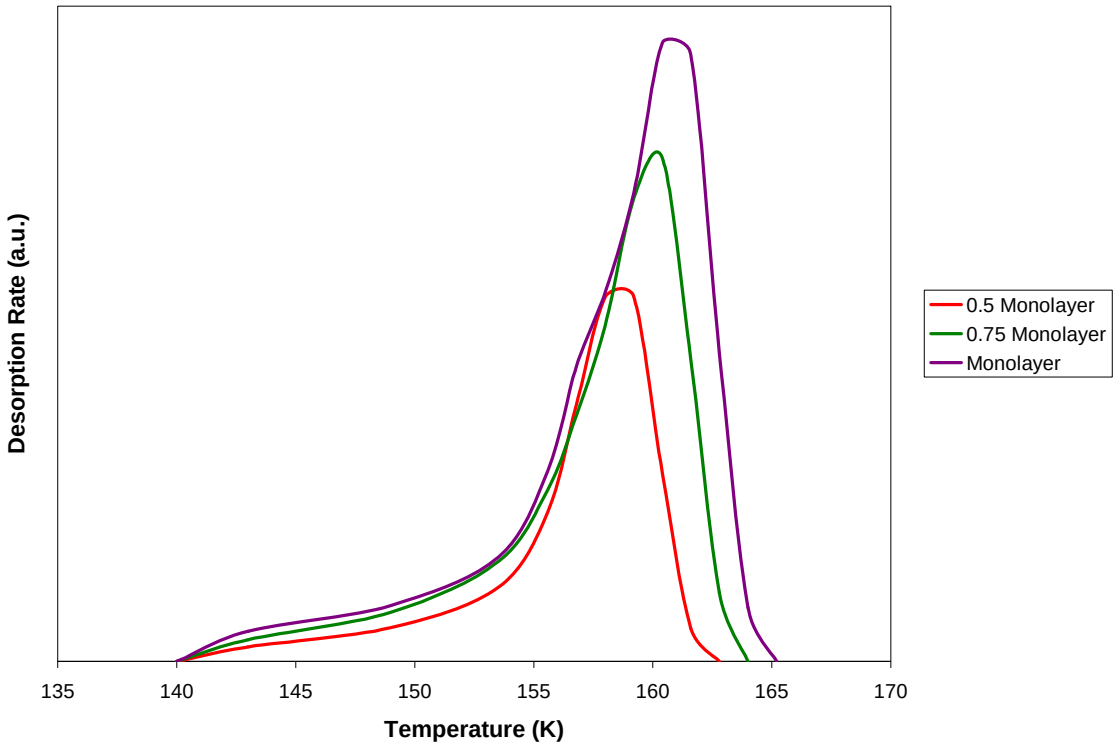

Figure **6-6**: TPD Profiles – Variable Initial Coverage, β = 0.6

Simulations were run for initial coverages of 0.5, 0.75, and a full monolayer. At this heating rate, the blocks chosen for the block averages ranged from 10 seconds at the beginning of the simulation to 2 seconds around the peak temperature, corresponding to the limitations of the mass spectrometer at this low heating rate. All coverages show a leading tail at the lowest temperatures and ranging almost 15 K before the steep initial rise of the TPD profile. The steep initial rise of all profiles overlap here, as they do in the butane and hexane results of Tait et al. [**10**] (shown in Figure **6-7**). Experimental TPD profiles of other alkanes on graphite also exhibit leading tails [**8-10**].

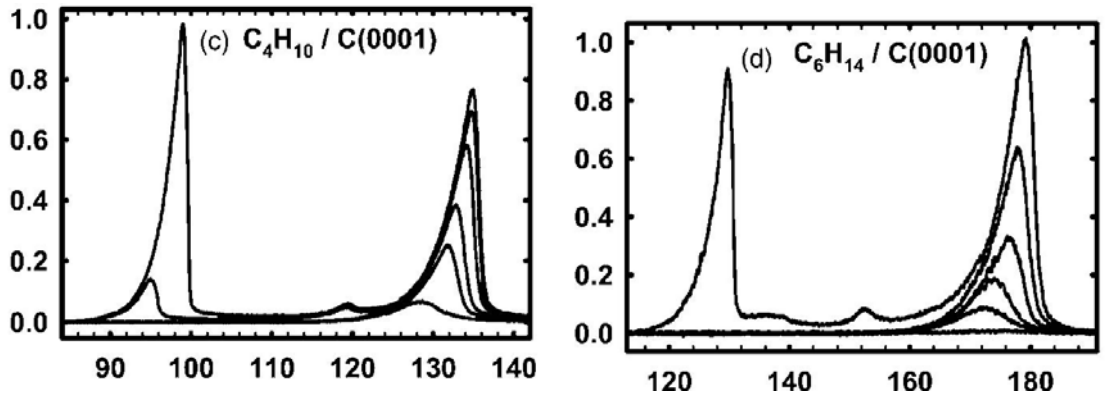

Figure **6-7**: TPD Profile for Butane and Hexane Desorbing from the Basal Plane of Graphite [**10**]

In their analysis of TPD profiles, Tait et al. assume that desorption is a first-order process [**10**]. In a strictly mathematically first-order process, this means that the peak temperature is independent of initial coverage [**33**]. However, in both the experimental results [**10**] and the simulation results, the peak temperature decreases slightly with decreasing initial coverage. The peak temperatures for each coverage are reported in Table **6-1**.

Table **6-1**: Peak Desorption Temperature for Pentane Desorbing from the Basal Plane of Graphite – Variable Coverage, $\beta = 0.6$ K/s

Coverage (ML)	Peak Temperature (K)
0.50	158.6
0.75	160.3
1.0	161.0

Simulations were also run at a heating rate of 0.5 K/s. The TPD profiles are shown in Figure **6-8**.

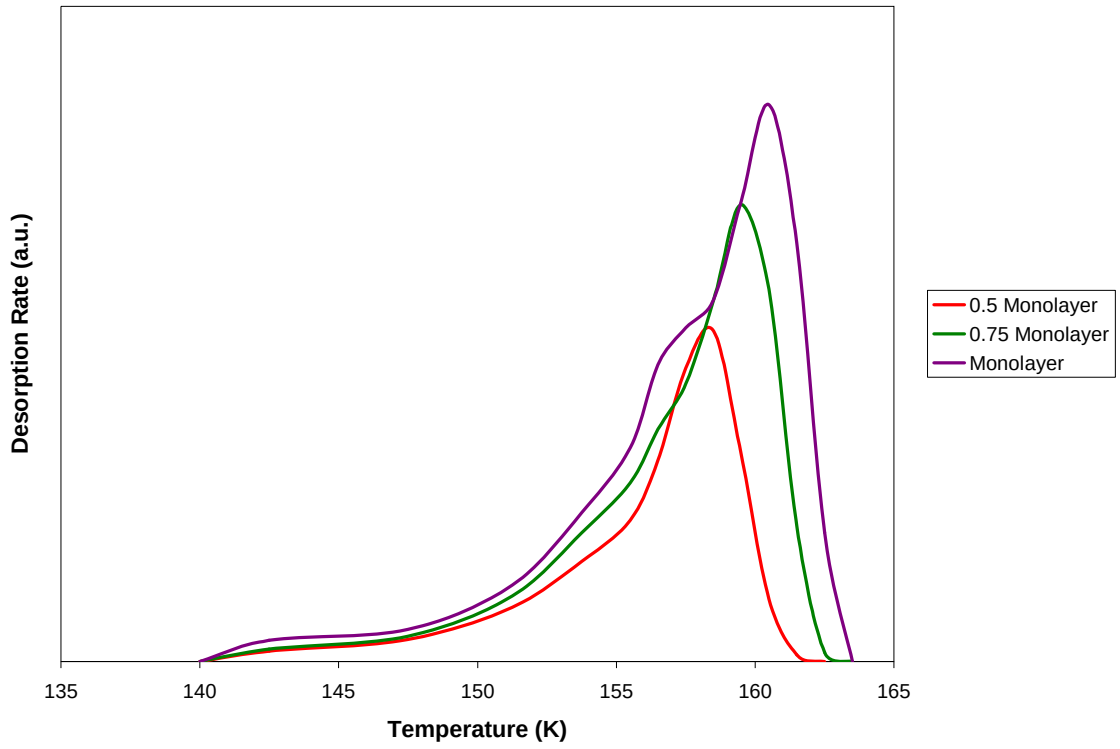

Figure **6-8**: TPD Profiles – Variable Initial Coverage, $\beta = 0.5$

This heating rate necessitates use of the same block averages as were used for a heating rate of 0.6 K/s. Again, these TPD profiles exhibit a leading tail at the lowest temperatures preceding the sharp initial rise. One prominent feature in this set of results is the shoulder on the monolayer peak. This shoulder does not appear to be an artifact of the simulation method since it is also observed in experimental TPD profiles of linear alkanes desorbing from metal surfaces [**8**]. Since both systems are dominated by van der Waals forces, there is no physical reason for these systems to have differently shaped TPD profiles. The shoulder appears at a coverage of around 0.57.

Study of the snapshots of the molecular orientation at this coverage offers a possible explanation for the shoulder. Figure **6-9** shows the structure of the pentane layer at the shoulder during the TPD simulation.

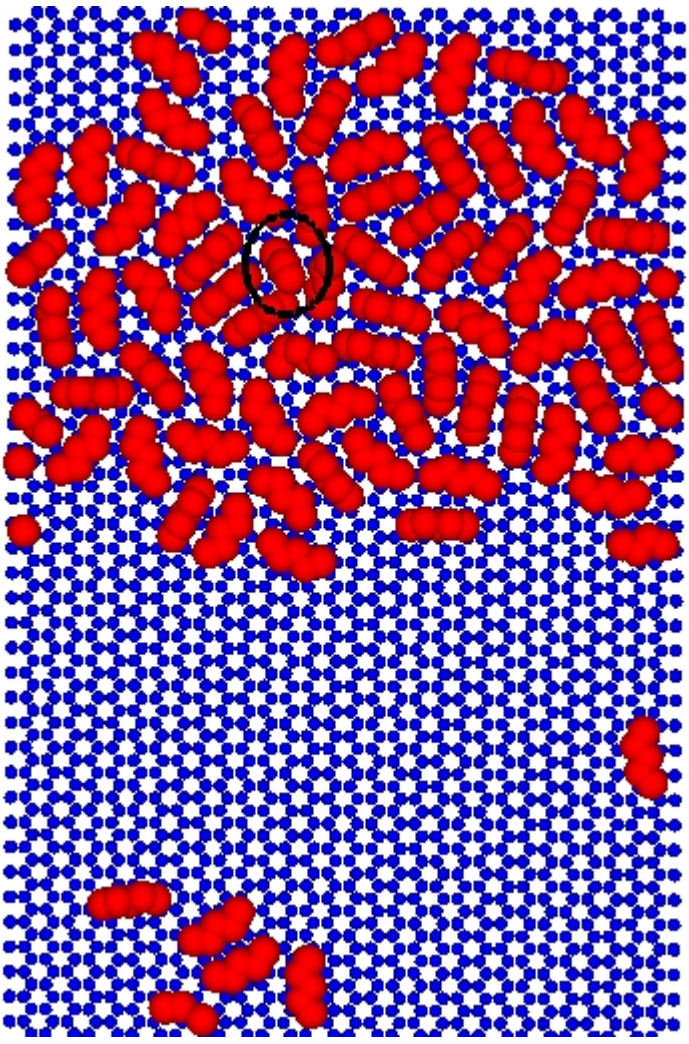

Figure **6-9**: Molecular Orientation – θ = 0.57 ML, β = 0.5 K/s

The molecule that is desorbing has been circled. As can be seen in Figure **6-9**, this molecule has many neighbors and thus large intermolecular interactions. It is also rolled so that the plane of the long axis of the molecule is perpendicular to the graphite surface. This decreases the molecule-surface interactions that act on the desorbing molecule.

Molecules crowd and order around the molecule. Due to this alignment, the entropy difference between the molecule adsorbed on the surface and the molecule in the gas phase following desorption is greater than would be expected when compared to molecules oriented randomly on the surface.

As in the case of β=0.6, the peak temperature decreases slightly with decreasing initial coverage. These temperatures are summarized in Table **6-2**.

Table **6-2**: Peak Desorption Temperature for Pentane Desorbing from the Basal Plane of Graphite – Variable Coverage, β = 0.5 K/s

Coverage (ML)	Peak Temperature (K)
0.50	158.4
0.75	159.5
1.0	160.5

6.3 TPD with Variable Heating Rate

Additional TPD simulations were also run with an initial coverage of one monolayer and heating rates of 0.5, 0.6, 2.0, and 5.0 K/s. The profiles for the simulations are found in Figure **6-10**.

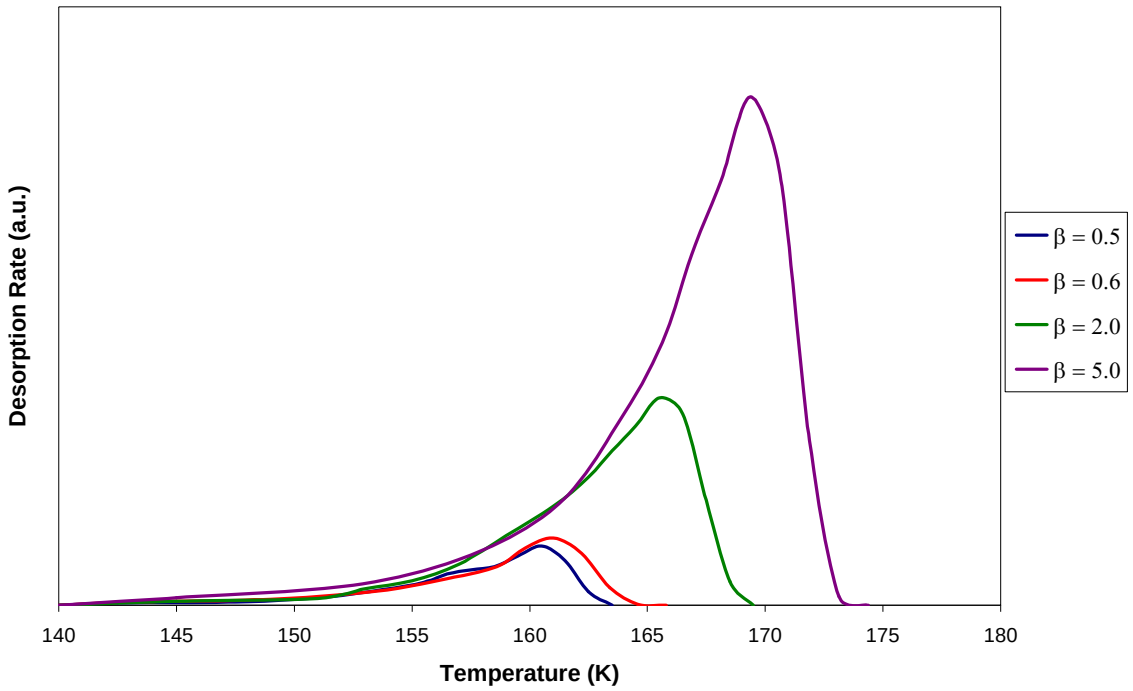

Figure **6-10**: TPD Profiles – Variable Heating Rate, Monolayer Initial Coverage

The features for the higher heating rate TPD profiles are much the same as the lower heating rate profiles for the monolayer discussed in Section **6.2**. The long leading tail persists, even at the high heating rates.

The blocks for block averages are smaller at the higher heating rates, because of the faster time resolution at those heating rates. For a heating rate of 2.0 K/s, the blocks ranged in size from 5 seconds at the beginning of the simulation to 0.5 seconds near the peak temperature. A heating rate of 5.0 K/s required even smaller blocks, ranging from 1 second at the beginning of the simulation to 0.25 seconds near the peak temperature.

The peak temperatures for the variable heating rate simulations are given in Table **6-3**.

Table **6-3**: Peak Desorption Temperature for Pentane Desorbing from the Basal Plane of Graphite – Variable Heating Rate, Monolayer Initial Coverage

Heating Rate (K/s)	Peak Temperature (K)
0.5	160.5
0.6	161.0
2.0	165.5
5.0	169.4

These results allow for a direct comparison to experimental data. In their work on the desorption of varying length alkane chains, Paserba and Gellman report a peak temperature of 164 K for the desorption of pentane from graphite at a heating rate of 2.0 K/s [**5**]. We report a peak temperature of 165.5 K for the same system and heating rate.

The variable heating rate results also shed light on the origin of the shoulder at low heating rates. As is shown in Figure **6-11**, the TPD profile where β=0.5 contains a prominent shoulder, while the TPD profile where β=5.0 does not.

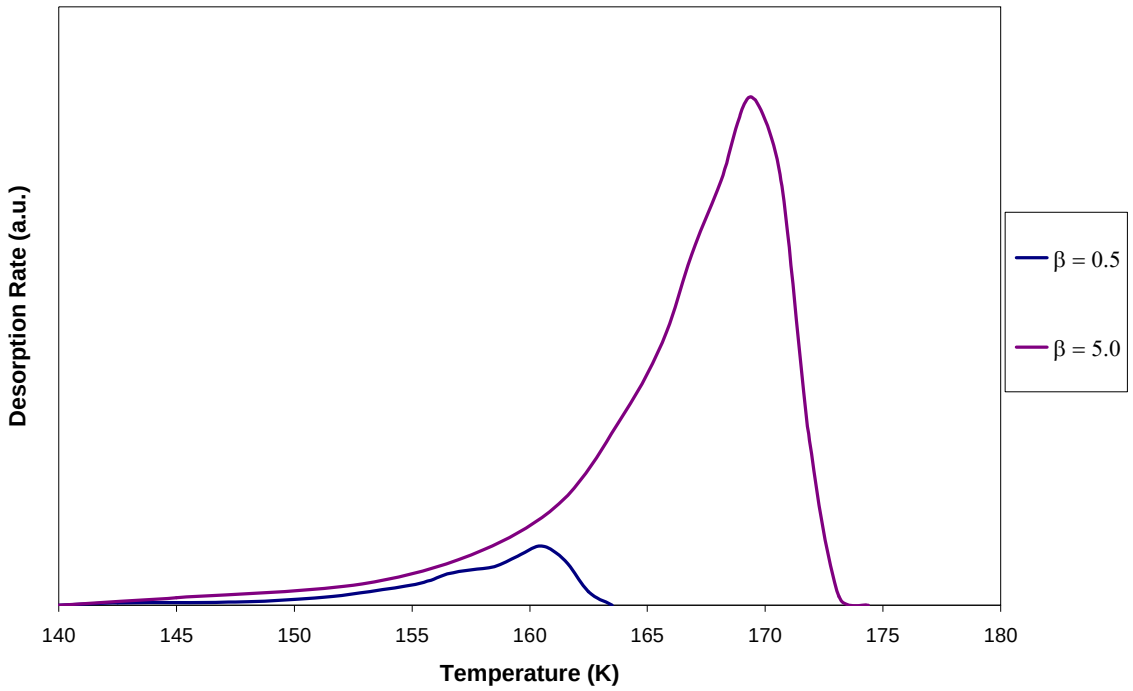

Figure **6-11**: TPD Profiles – β = 0.5 K/s and β = 5.0 K/s, Monolayer Initial Coverage

As discussed in Section **6.2**, the shoulder at β=0.5 occurs when the coverage is around 0.57. At that heating rate, the temperature corresponding to that coverage is around 158 K. At a heating rate of β=5.0, a coverage of 0.57 occurs at a temperature around 167 K. A snapshot of the layer during the TPD simulation at this coverage and temperature (Figure **6-12**) shows a layer with far less order.

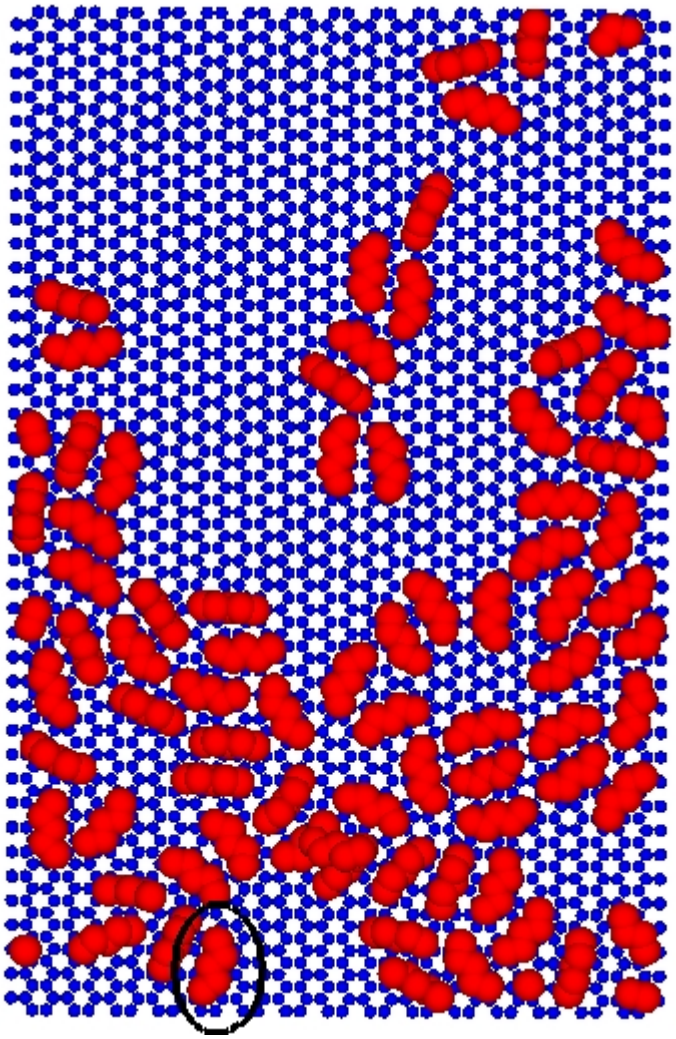

Figure **6-12**: Molecular Orientation – θ = 0.57, β = 5.0 K/s

The molecule that is circled is again the one that is in the process of desorbing. This molecule is lying flat with the plane of the backbone parallel to the graphite surface. It has fewer neighbors and thus lower intermolecular interactions. The entropy gained upon desorption is less than the entropy gained by the molecule desorbing at the lower heating rate from a different desorption environment (Figure **6-9**). Thus, it is the desorption environment and the entropy changes associated with it that cause the presence of the shoulder at low heating rates.

Using variable heating data from the simulations, simulated TPD profiles are analyzed in the same manner as experimental TPD profiles. Desorption energy and prefactors obtained from the analyses can therefore be compared. This analysis is based on Eq. **6.5** and discussed extensively in Section **6.1**. It assumes that the desorption process is first-order. Figure **6-13** shows the plot used to determine desorption energy.

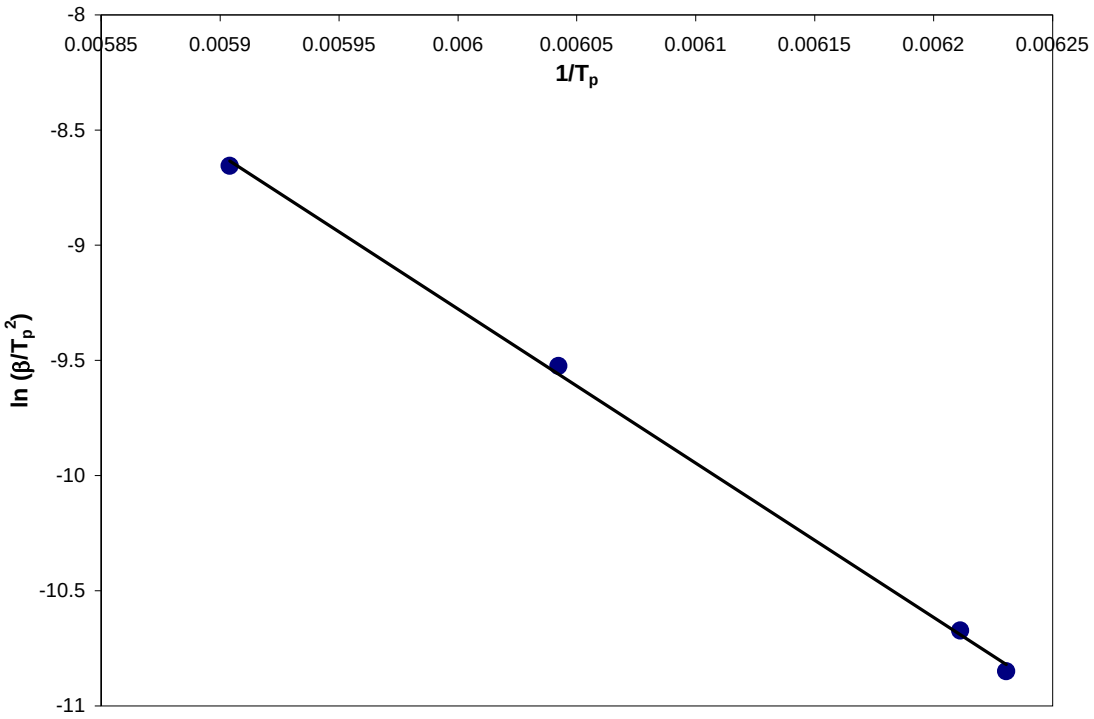

Figure **6-13**: Variable Heating Rate Plot of $\ln(\beta/T_p^2)$ versus $1/T_p$

The slope of the line yields a desorption energy of 55.7 kJ/mol with a standard deviation of 5.0 kJ/mol. This value for the desorption energy is then used in Eq. **6.5** along with the peak temperatures and corresponding heating rates. Prefactors from this analysis are given in Table **6-4**. The average value of the prefactor from this analyis is $10^{17.2}$. This is in line with the values of the prefactor reported in [**10**].

Table **6-4**: Prefactors Calculated from Variable Heating Rate Data

Heating Rate (K/s)	$Log_{10}(\nu)$
0.5	17.2299
0.6	17.2501
2.0	17.258
5.0	17.2339

6.4 Role of Defects

Variable coverage simulations were also run at an initial coverage of 0.25 ML at β=0.6. These simulations are not consistent with the variable coverage simulations at higher initial coverages or experimental data. As can be seen in Figure **6-14**, the profile for an initial coverage of 0.25 ML is at much lower temperatures than is found in experiment. The peak also exhibits a much narrower profile than would be expected.

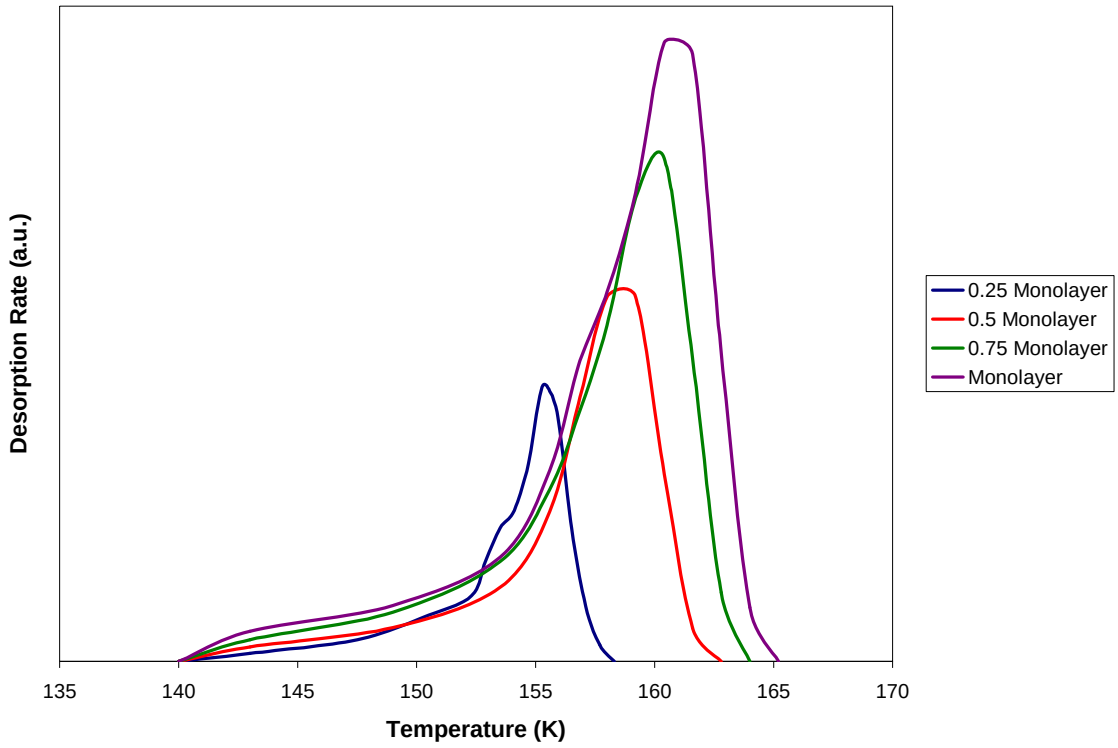

Figure **6-14**: TPD Profiles – Variable Coverage (Including 0.25 ML), β = 0.6 K/s

We hypothesize that these differences are caused by defects in the graphite surface in the experiments. Tait et al. [**10**] show that the desorption energy of butane desorbing from the basal plane increases rapidly as the coverage decreases below 0.2 ML (Figure **6-15**).

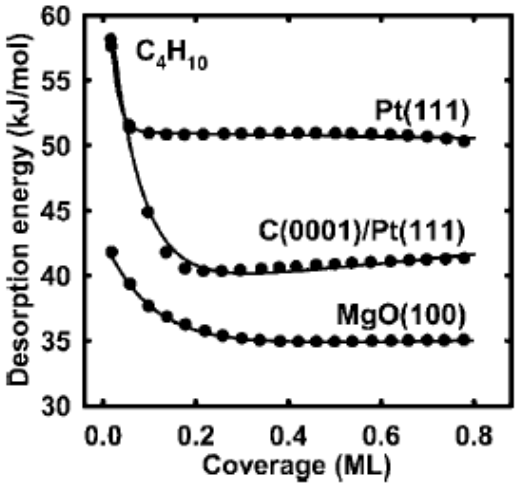

Figure **6-15**: Desorption Energy as a Function of Coverage [**10**]

Alkane molecules will adsorb more strongly to defects in the graphite surface and thus require higher energies for desorption. As a result, these molecules are the last ones to desorb from the surface. In the TPD simulations, the graphite surface is modeled as a perfect crystal with no defects. Since the last alkane molecules that desorb from the simulation are going to have fewer neighbors (and lower intermolecular interactions) they will desorb at lower energies than molecules at higher coverages. Defects in the graphite surface would create many more desorption environments at higher energies. This would shift the TPD profile for 0.25 ML to higher temperatures due to the higher desorption energies, and broaden it due to multiple desorption environments at these higher energies.

6.5 Conclusions and Recommendations

We have successfully simulated TPD with an accelerated MD scheme. This is, to our best knowledge, the first time that TPD has been successfully simulated on a molecular level. The simulations are consistent with previously published experimental data. We put forth an explanation for the shoulder on the TPD profile that is seen in both our simulations and experimentally at low heating rates. Entropic forces appear to be the driving force for desorption in certain regions of the TPD profile, including the long leading tail and the shoulder seen at low heating rates. At low coverages, the role of defects is a major one which affects both the position of the TPD peak and its shape. The simulated TPD profiles are interpreted in the same manner as experimental profiles. This produces a desorption energy and prefactor that are consistent with experimental results. However, the insight provided by the simulations shows that the traditional Redhead analysis appears to be insufficient. While the peaks may look first-order, they are only quasi-first-order. The assumption that the prefactor is coverage independent is a faulty one. Redhead analysis also fails to predict the decrease in rate with coverage due to entropic forces.

The following suggestions for simulations will address some of these open issues. A model for the graphite surface that does not assume a perfect crystal would help to examine the role of defects in the desorption process. Alternately, a potential could be added to the current model of the graphite surface to create defects in the perfect crystal potential. A study examining the role of chain length in addition to coverage would provide interesting insights into the role of entropy in the desorption process. As has

been shown at the single molecule limit, entropy plays an important role. Entropy differences in a layer of longer chain molecules with increased internal entropy would be even more pronounced.

In addition, there are other methods that can be used to extract desorption energies and prefactors from a TPD spectrum [**36**], including coverage-dependent values. Applying these methods to current data and data at a larger range of heating rates would provide a comparison to the coverage-dependent values determined in the fixed-coverage simulations presented in Chapter 5.

A complete theoretical study would be necessary to improve the analysis of TPD profiles. It is clear from the results in this thesis that the prefactor and desorption energy are coverage dependent. To include this effect, it would be necessary to quantatively relate desorption energy and prefactor to coverage. Also, the desorption process is not first-order as is assumed in most of the analyses. Instead, it appears that the desorption order changes depending on the desorption environment. Various mathematical forms for the kinetics of the desorption process, other than a simple power law, can be studied and fit to experimental or simulated data. Important features that are ignored in the first-order desorption analysis, such as the shoulder at low heating rates, should be included in the new form for the kinetics.

Bibliography

1. E.K. Grimmelmann, J.C. Tully and E. Helfand, *J. Chem. Phys.*, **74**, 5300 (1981).

2. A.F. Voter and J.D. Doll, *J. Chem. Phys.*, **80**, 5814 (1984).

3. A.F. Voter, *Phys. Rev. Lett.*, **78**, 3908 (1997).

4. R.A. Miron and K.A. Fichthorn, *J. Chem. Phys.*, **119**, 6210 (2003).

5. K.R. Paserba and A.J. Gellman, *J. Chem. Phys.*, **115**, 6737 (2001).

6. A.R. Bishop, G.S. Girolami and R.G. Nuzzo, *J. Phys. Chem. B*, **104**, 754 (2000).

7. K.A. Fichthorn and R.A. Miron, *Phys. Rev. Lett.*, **89**, 196103 (2002).

8. R.Z. Lei, A.J. Gellman and B.E. Koel, *Surf. Sci.*, **554**, 125 (2004).

9. S.L. Tait, Z. Dohnálek, C.T. Campbell and B.D. Kay, *J. Chem. Phys.*, **122**, 1 (2005).

10. S.L. Tait, Z. Dohnálek, C.T. Campbell and B.D. Kay, *J. Chem. Phys.*, **125**, 234308 (2006).

11. K.E. Becker and K.A. Fichthorn, *J. Chem. Phys.*, **125**, 184706 (2006).

12. D.S. Martin, P. Weightman and J.T. Gauntlett, *Surf. Sci.*, **424**, 187 (1999).

13. T. Arnold, R.K. Thomas, M.A. Castro, S.M. Clarke, L. Messe and A. Inaba, *Phys. Chem. Chem. Phys.*, **4**, 345 (2002).

14. Z. Wu, S.N. Ehrlich, B. Matthies, K.W. Herwig, P. Dai, U.G. Volkmann, F.Y. Hansen and H. Taub, *Chem. Phys. Lett.*, **348**, 168 (2001).

15. F. Kruchten, K. Knorr, U.G. Volkmann, H. Taub, F.Y. Hansen, B. Matthies and K.W. Herwig, *Langmuir*, **21**, 7507 (2005).

16. J.S. Raut, D.S. Sholl and K.A. Fichthorn, *Surf. Sci.*, **389**, 88 (1997).

17. F.Y. Hansen, J.C. Newton and H. Taub, *J. Chem. Phys.*, **98**, 5 (1993).

18. M. Krishnan, S. Balasubramanian and S. Clarke, *J. Chem. Phys.*, **118**, 5082 (2003).

19. C.L. Pint, *Phys. Rev. B*, **73**, 045415 (2006).

20. P.A. Redhead, *Vacuum*, **12**, 203 (1962).

21. W.L. Jorgensen, D.S. Maxwell and J. Tirado-Rives, *J. Amer. Chem. Soc.*, **118**, 11225 (1996).

22. W.A. Steele, *Surf. Sci.*, **36**, 317 (1973).

23. H.-Y. Kim and W.A. Steele, *Phys. Rev. B*, **45**, 6226 (1992).

24. H.C. Andersen, *J. Comput. Phys.*, **52**, 24 (1983).

25. P.Y. Bruice, *Organic Chemistry*, Prentice Hall: Upper Saddle River NJ, 1998.

26. H.J.C. Berendsen, J.P.M Postma, W.F. van Gunsteren, A. DiNola and J.R. Haak, *J. Chem. Phys.*, **81**, 3684 (1984).

27. M.P. Allen and D.J. Tildesley, *Computer Simulation of Liquids*, Oxford University Press: New York, 2007.

28. P. Hänngi, P. Talkner and M. Borkovec, *Rev. Mod. Phys.*, **62**, 251 (1990)

29 S. Arrhenius, *Z. Phys. Chem.*, **4**, 226 (1889).

30. L. Farkas, *Z. Phys. Chem.*, **125**, 236 (1927).

31. H. Eyring, *J. Chem. Phys.*, **3**, 107 (1935).

32. R.A. Miron. "A Journey across Time Scales: Accelerated Atomistic Simulation of Surface Growth." Ph.D. thesis, The Pennsylvania State University, (2004).

33. R.I. Masel, *Principles of Adsorption and Reaction on Solid Surfaces*, Wiley: New York, 1996.

34. B. Matthies, Ph.D. thesis, University of Missouri-Columbia, 1999.

35. NIST Center for Neutron Research, *Neutron News*, **3**, 29 (1992).

36. J.B. Miller, H.R. Siddiqui, S.M. Gates, J.N. Russell, Jr, J.T. Yates, Jr., J.C. Tully and M.J. Cardillo, *J. Chem. Phys.*, **87**, 6725 (1987).

VITA

Kelly E. Becker

Education

Ph. D., Chemical Engineering — December 2008
Graduate Minor in High Performance Computing
The Pennsylvania State University, University Park, PA
B.S. Chemical Engineering — May 2002
Minor in Mathematics
State University of New York at Buffalo, Buffalo, NY

Publications

K.E. Becker and K.A. Fichthorn. "Accelerated molecular dynamics simulation of thermal desorption of n-alkanes from the basal plane of graphite", *J. Chem. Phys.* **125**, 184706 (2006).
K.A. Fichthorn, K.E. Becker and R.A. Miron. "Molecular simulation of temperature-programmed desorption," *Catalysis Today* **123**, 71 (2007).

Honors

APS Division of Chemical Physics Graduate Student Travel Award (2007)
George and Ruth S. Robb Fellowship (2004)
Allied Signal Scholarship Award (2002)
Motorola Senior Scholar Award (2002)

Conference Presentations

K.E. Becker and K.A. Fichthorn. "Accelerated Molecular Dynamics Simulation of Alkane Desorption." AIChE National Meeting, Salt Lake City, UT (2007).
K.E. Becker and K.A. Fichthorn "Accelerated Molecular Dynamics Simulation of Protein Folding." AIChE National Meeting, Salt Lake City, UT (2007).
K.E. Becker and K.A. Fichthorn. "Accelerated Molecular Dynamics Simulation of Alkane Desorption." Poster, Dynamics at Surfaces Gordon Research Conference, Andover, NH (2007).
K.E. Becker and K.A. Fichthorn. "Accelerated Molecular Dynamics Simulation of Thermal Desorption." APS National Meeting, Denver, CO (2007).
K.E. McLaughlin and K.A. Fichthorn. "Accelerated Molecular Dynamics Simulation of Alkane Desorption." APS National Meeting, Baltimore, MD (2006).
K.E. McLaughlin and K.A. Fichthorn. "Accelerated Molecular Dynamics Simulation of Thermal Desorption: n-Alkanes on Graphite." AIChE National Meeting, Cincinatti, OH (2005).
K.E. McLaughlin and K.A. Fichthorn. "Accelerated Molecular Dynamics Simulation of Thermal Desorption." Poster - IPAM Workshop: Multiscale Modeling, Los Angeles, CA (2005).